Role of Fitted Reaction Rates in Predicting Thrombin Production

Wenrui Hao[1] and Guang Lin[2]and Zhiliang Xu[3]and Elliot Rosen[4] and Andrew Sommese*[3]and Mark Alber*[3,5]

[1] Mathematical Biosciences Institute, The Ohio State University, Columbus, OH, 43210
[2] Computational Mathematics Group, Pacific Northwest National Laboratory, 902 Battelle Boulevard, Richland, WA 99352
[3] Department of Applied and Computational Mathematics and Statistics, University of Notre Dame, Notre Dame, IN 46556
[4] Department of Medical and Molecular Genetics, Indiana University School of Medicine
[5] Department of Medicine, Indiana University School of Medicine

Email: Wenrui Hao - hao.50@mbi.osu.edu; Guang Lin - guang.lin@pnnl.gov; Zhiliang Xu - zxu2@nd.edu; Elliot Rosen - edrosen@iupui.edu; Andrew Sommese*- sommese@nd.edu; Mark Alber*- alber@nd.edu;

*Corresponding author

Abstract

Background: The blood coagulation system is composed of a complex network of chemical reactions. This network can be modeled by the Hockin-Mann et al theoretical model.

Results:

We have developed a systematic approach to analyzing high-dimensional stoichiometric biological-reaction network models represented by systems of ordinary differential equations (ODEs) with parameters obtained by data-fitting. In this approach, A new algorithm based on numerical algebraic geometry is introduced to compute steady state solutions to rank-deficient systems with different initial conditions. Then the variance decomposition based on the sensitivity analysis and Morris design method is used to rank the significance of the reaction rate constants obtained by data-fitting on affecting outputs of the models. Subsequently, the sparse grid probabilistic collocation method (SGPCM) is employed to quantify how uncertainties of these reaction rates influence the model outputs.

Conclusions: We present a general framework for analyzing high-dimensional biological reaction network models represented by system of ODEs with a large number of parameter sets. We also show that that SGPCM can achieve much faster convergence than classic Monte Carlo method with much lower computational cost.

Specifically, we systematically analyzed the Hockin-Mann model of the extrinsic (TF mediated) coagulation

pathway model using this framework. We ranked the significance of the 16 data-fitted reaction rates of the model on affecting the total thrombin production and found that the reaction rate k_{14}, which is related to factor IX, plays the most important role in determining the thrombin generation. Finally, we ranked the importance of all reaction rate constants using sensitivity analysis to identify critical threshold levels for factors VIII and IX to suggest how to alter either concentrations of these factors or reaction rates associated with them for hemophilia therapies targeting these factors. Using simulations, we suggest that increasing the value of k_{14} or decreasing the concentration of factor X would be feasible for hemophilia patients with bleeding disorder.

Introduction

It is becoming increasingly vital to combine laboratory research with mathematical modeling and computer simulation to get additional insight into biological processes [1, 2, 12, 23, 37, 43, 45, 51, 57, 58, 60, 63, 66]. In the process of model development, conceptual model is firstly established by making some simplifying assumptions. Then, it is implemented mathematically and analyzed using theoretical approaches or numerical methods. Meanwhile, experiments are used to estimate model parameters and to calibrate and validate the model. However, due to errors in experimental measurements, there always exists uncertainty in parameter estimation. This uncertainty includes model simplifications, computational errors coming from numerical schemes, and random local rules in Monte carlo simulations. The situation could become even worse if certain parameter values may be impossible to measure using current experimental techniques, and to test a range of parameter values. Thus, identifying the sensitivity and uncertainty of the model parameters becomes essential for using models to make predictions and to explore biological hypotheses.

Recently, many methods have been developed for analyzing sensitivity of chemical/biological reaction networks. These include Morris method [46], the sparse grid probabilistic collocation method (SGPCM) [40, 41, 67], pathwise sensitivity analysis methods [50] and many other methods. However, many of these methods have difficulty in studying high-dimensional models.

In this paper, we introduce a new general framework for quantifying uncertainty, analyzing the parameters, and determining steady states of chemical/biological reaction network models in the form of systems of ordinary differential equations (ODEs) (see Fig. 1), and demonstrate this approach by using it to analyze a specific example, Hockin-Mann's model [28] of blood coagulation.

Using this framework, we first compute the steady state solution structures and characteristics of a ODE model using a newly developed numerical algebraic geometry method, which is capable of finding all steady

state solutions for arbitrary initial conditions. The steady state solutions are known to be dependent on the initial conditions and reaction rates. We demonstrate that our new algorithm is able to compute all steady states of models represented by a singular sparse polynomial system, and with a large number of variables.

We then used two stochastic sensitivity analysis tools, namely, Morris method [46] based on Monte Carlo (MC) simulation and sparse grid collocation based on SGPCM approach, to rank the importance of the reaction rate constants of the model. We show that the results obtained by these two methods are consistent. However, the SGPCM has higher order of convergence than the Morris method, which is a classical method on sensitivity analysis, and depends on MC method. In addition, the SGPCM can also provide the effects between reaction rates and initial concentrations of reactants respectively.

The SGPM is used in the end to quantify uncertainties of the model. We validate the result obtained by the SGPM with the one obtained by Monte Carlo to show that the SGPM can handle the high-dimensional model.

We examine the effectiveness of this computational framework by applying it to analyze a blood coagulation model, Hockin-Mann's model [28]. This model simulates blood coagulation reactions, one of the key processes controlling blood clot (or thrombus) formation. And proper blood clotting (or hemostasis) is critical to preventing hemorrhaging. Particularly, we explored the solution structures of the model, ranked the sensitivity and quantified the uncertainties of reaction rate constants of the model, which were determined by fitting computational results with empirical data.

Most of the therapeutic drugs treating hemophilia would vary one or two reaction rates or increase concentrations of certain coagulation factors to increase factor thrombin production. Using our sensitivity analysis results, we studied the effects of several hemophilia drugs (shown in Table 9) on the rate of thrombin production. Specifically, we predicted the threshold value of concentration of factor VIII (FVIII) in reducing the risk of bleeding disorder while keeping other blood coagulation factors at the normal levels of concentration. In this case, we predicted that it is sufficient to maintain the FVIII concentration to be 4.7% of its normal level .

Biological Background of Hockin-Mann's model

During the initial step of clot formation, resting platelets in blood are activated following adhesion to matrix proteins exposed from the damaged vessel wall. At the same time, blood borne factor VII binds with vessel wall tissue factor (TF) to form VIIa-TF complex (VIIa stands for activated factor VII) to initiate a complex set of blood coagulation reactions [47]. Coagulation reactions lead to the formation of thrombin

from prothrombin. Thrombin is efficient in activating platelets and also converts fibrinogen in blood to fibrin which self-polymerizes, forming a fibrin network that is a major structural component of the clot [29, 36].

Platelets lead to pro-thrombotic changes upon activation. These include the release of their contents of alpha and dense granules that contain coagulation factors and platelet activators, modification of the platelet surface to promote surface dependent coagulation reactions, and the activation of the integrin receptor gpIIaIIIb which can bind fibrin(ogen), von Willebrand Factor (vWF) and vitronectin, enabling these molecules to bind adjacent platelets and increase platelet to platelet adhesivity.

In parallel with platelet activation, VIIa-TF complex formed by factor VII and TF binding catalyzes the conversion of factor X to Xa directly or via a IXa-VIIIa intermediary step. Activated factor Xa combines with its protein cofactor, factor Va, on the surfaces of platelets to form prothrombinase (Va-Xa complex) which, in turn converts prothrombin (II) to thrombin (IIa) through an intermediate meizothrombin (mIIa). Transient mIIa is rapidly converted to IIa in the presence of factor Va and pro-coagulant lipids. Factor V is activated to its active form Va by both factor Xa and IIa. Thrombin activates platelets, converts fibrinogen to fibrin and activates factors V, VIII, and XI which provide a positive feedback loop propagating the production of thrombin. Thrombin is also a potent activator of resting platelets and thus mediates recruitment of resting platelets flowing nearby in the blood. The activated platelets provide a procoagulant surface that promotes coagulation enzyme activity. The formation and activity of VIIIa-IXa and Va-Xa complexes are dependent on the availability of phospholipid binding sites, which are only expressed on the surfaces of activated platelets [1, 9, 28, 34–36].

The coagulation process is also regulated by inhibitors of coagulation reactions. TFPI binds VIIa-TF with factor Xa resulting in inhibition of the coagulation initiation reaction. ATIII inactivates several coagulation factors including thrombin, factor IXa and factor Xa. In addition, thrombin also initiates a negative feedback loop that possibly limits continued thrombin production by binding thrombomodulin on endothelial cells and activating Protein C. Activated Protein C inactivates factor Va and factor VIIIa which are required for continued thrombin generation. The activation of the PC anticoagulant pathway is initiated after thrombin generation begins, suggesting that it might provide a negative feedback mechanism to limit growth of a developing thrombus. Additionally, activated platelets release endothieliel cell selective adhesion molecule (ESAM) which interferes with platelet to platelet adhesion. Presumably the release of anti thrombotic components at late stages of platelet activation might stop continued thrombus growth [13, 18, 28, 32, 33].

Prior to the Hockin-Mann's model [28], Mann's group proposed a mathematical model in the form of system of ordinary differential equations [32, 33] to describe the TF-initiated pathway reactions based on

in vitro experiments. The work in [32, 33] provided a good approximation of empirical data for blood clot formation. Subsequently, this model [32, 33] was improved by including blood anticoagulants tissue factor pathway inhibitor (TFPI) and antithrombin III (AT-III), and detailed descriptions of coagulation enzyme activities [28]. The new model (termed Hockin-Mann's model thereafter) accurately predicted the nonlinear dependence of thrombin generation on the tissue factor and has been widely used to understand how various coagulation factors interact with each other and how variations of these factors affect thrombin production [9, 10, 13, 18, 30, 35, 68].

Despite wide applications of Hockin-Mann's model [28] and the model described in [32, 33], structures, characteristics of steady state solutions of theses models, sensitivity of the models, and uncertainty of parameter values have yet to be discussed. So far, only Lo *et al.* conducted kinetic Monte Carlo simulations [42] using the reaction network described in this model [28] to allow them to accurately simulate blood coagulation with low concentrations of blood zymogens and enzymes, which deterministic models often fail to predict. Specifically, rates of thrombin production were studies using low TF concentrations. Simulations revealed that 0.2pM TF was the critical concentration to cause 50% of reactions containing 3-fold diluted whole blood to generate 0.05 U/ml thrombin by 1 hour [42]. Additionally, Luan *et al.* [43] applied sensitivity analysis to their model of coagulation reactions to identify fragile sites. Using parameter values from the literature, reactions were identified where small changes in parameter values would have dramatic effects on thrombin generation and platelet activation. This analysis [43] identified reactions involving an interaction of factors IX and VIII as the most sensitive reactions to small fluctuations of relevant parameters.

Results

Mathematical and computational framework for analyzing biological reaction networks

We present a general approach to compute the steady states and analyze importance of parameters, and provide diagram of different stages in the process in Figure 1 and Box 1. We demonstrate this general approach by analyzing Hockin-Mann's model.

Box 1 Computing steady states and analyzing the effects of parameters for a general reaction network model.

1 numerical algebraic geometry (NAG) introduces a novel paradigm of computing steady states. Especially, we present a new algorithm for the rank-deficient polynomial system which is derived from the reaction network model;

2 uncertainty quantification (UQ) and sensitivity analysis (SA) estimate and identify parameters in the mathematical model. In particular, we employ SGPCM, Morris method to analyze the effects of parameters;

3 Adjusting the most sensitive parameters and comparing with the existence therapy provide threshold values of sensitive parameters for a given disease.

Analysis of steady state solutions

Using **Algorithm 2** described in **Methods** to solve the steady state system of the blood coagulation model, we found 88 equilibrium (steady state solutions) for Hockin-Mann's model based on initial conditions from [28], and that all equilibriums are determined by linear and quadratic equations shown in Table 1. In particular, Thrombin IIa (x_{13}) and meizothrombin mIIa (x_{16}) are free variables, and linearly depend on the initial condition (linear equations), reaction rates, and values of other species such as TF=VIIa=X (x_{17}), TF=VIIa=Xa (x_{19}) as well as Xa=TFPI (x_{20}) (quadratic equations). Moreover, the constants shown in linear equations, such as 3.3383×10^{-9} and 2.33×10^{-10}, are determined by initial conditions. Quadratic equations account for effects of reaction rates k_i.

Next, linear stability analysis is used to explore the steady state solution and study the matrix eigenvalue problems of the linearized system. Moreover, the nonlinear stability analysis is applied to a simplified steady state solution.

Linear stability

We consider the local stability of steady state solutions. Assuming that $x_i = x_i^s + \epsilon x_i^1 + O(\epsilon^2)$ for $i = 1, \cdots, 34$, where x_i^s is the i-th component of steady state solutions we obtained using the method described in section **Methods**, and x_i^1 is the first order term by Taylor expansion at the steady states. By substituting x_i into Eq. (7) in Appendix B, and dropping $O(\epsilon^2)$ and higher order terms, the linearized system is obtained and shown in Appendix D. The linearized system can be written as

$$\frac{d\mathbf{x}^1}{dt} \;=\; A(\mathbf{x}^s)\mathbf{x}^1,$$

which implies that $\mathbf{x}^1 = e^{A(\mathbf{x}^s)t}$. If all the eigenvalues of $A(\mathbf{x}^s)$ are non-positive, the steady state solution $\mathbf{x}^s$ is stable. Since the matrix $A(\mathbf{x}^s)$ linearly depends on $\mathbf{x}^s$, we obtain the following formula

$$A(\mathbf{x}^s) \;=\; \sum_{i=1}^{34} A_i x_i^s,$$

where A_i is a real matrix and independent on x_i^s.

All of the maximum eigenvalues of A_i are negative and are shown in Table 2. Therefore all eigenvalues of $A(\mathbf{x}^s)$ are also negative for any $\mathbf{x}^s$ with positive components. Thus, the linearized system corresponding to any steady state solution is stable. Then, we switch our attention to check the nonlinear stability of solutions shown in Table 1.

Nonlinear stability

Among these 88 steady states, we analyze one steady state, which is "close" to results obtained by solving Hockin-Mann's model [28] using the time marching method. And rest of steady states can be analyzed in a similar way. Specifically, this steady state solution is obtained by the following manner: combining with the time marching result from [28], the free variables in Table 1 are set to zero except the thrombin (x_{13}), meizothrombin (x_{16}) and TF=VIIa=X (x_{17}). Thus, a simplified steady state solution is obtained in Table 3. By solving the polynomial system with respect to variables x_{13}, x_{16} and x_{17} with Bertini [4], we get one real positive solution as follows

$$x_{13} = 2.99990 \times 10^{-8}, x_{16} = 2.32829 \times 10^{-14}, x_{17} = 1.03445 \times 10^{-12}.$$

Then x_{19} and x_{20} can be obtained by substituting x_{16} and x_{17} into the linear equations in Table 3. This solution shows that total thrombin concentration is related with the complex TF=VIIa=X (x_{17}). In particular, equation $k_{18}x_{17} + k_{25}x_{17} - k_{19}x_{16}x_{13} = 0$ reveals the fact that TF=VIIa=X links with thrombin and meizothrombin through IXa=VIIIa in No. 11 and 15 chemical equations. Moreover, TF=VIIa=X also affects the amount of TF=VIIa=Xa (x_{19}) and Xa=TFPI (x_{20}) together with meizothrombin (linear equations). We note that the difference between the solution computed by the time marching method and the steady state solution that we choose to analyze is smaller than 10^{-7} in L_1 norm. Relative differences of the nonzero components are shown in Table 4.

Nonlinear stability analysis is accomplished by the following steps: applying random perturbations (a sequence ϵ_n in Table 5) to the steady state solution gives initial conditions for the initial value problem shown in Appendix B; Runge-Kutta method is used to solve this initial value problem numerically. The

results, summarized in Table 5, demonstrate that the steady state solution is non-asymptotically stable. In this case, the system moves away in a small region from the steady state solution after introducing small disturbances. Therefore, this chemical reaction network depends sensitively on the initial condition and the reaction rates.

Steady states for different initial conditions

Since initial conditions determine linear equations by generating an augmented system and play an important roll in computing steady states, we consider different initial conditions from [35], which respond in a threshold manner to changes in the availability of particular surface binding sites for enzymes and zymogens. Using the **Algorithm 2**, we obtained steady state solutions and show them in Table 6. The free variables in Table 6 are set to zero, and then a specified steady state solution is obtained in Table 7. By solving the polynomial system in Table 7, we get two positive real solutions as follows:

$$x_{13} = 4.99656 \times 10^{-7}, x_{16} = 4.12563 \times 10^{-13}, x_{17} = 3.43569 \times 10^{-10}; \tag{1}$$

$$x_{13} = 4.46036 \times 10^{-7}, x_{16} = 7.25906 \times 10^{-11}, x_{17} = 5.39634 \times 10^{-8}. \tag{2}$$

In these two steady state solutions, (1) can be obtained by a time marching method based on the given initial conditions, while (2) can not be obtained by the time marching approach. However, (2) is also stable since it can come back to itself by giving small perturbation to (2) by time-marching. In many biological systems, there exists multiple equilibriums even for a given initial condition. Moreover, a small perturbation to an equilibrium can approach the equilibrium by time-marching indicates that the equilibrium is stable. Therefore, our method is competitive to find multiple steady state solutions.

Comparing Tables 3 and 7, polynomial equations have different coefficients. Therefore, these steady state solutions show a very sharp transition in predicting thrombin production as the initial conditions vary. Changes of these initial conditions induce an increase of thrombin concentration (x_{13}) by 10 times. Moreover, meizothrombin concentration (x_{16}) is also increased by 10 or even 1000 times. Our results are consistent with that of [35] and [42]. In fact, initial TF density is known to change the total thrombin significantly when a vessel is injured. A threshold dependence on TF concentration is found in the experiments by Veer and Mann [65]. Additionally, numerical study for low TF density was carried out in [42] by using Kinetic Monte Carlo simulation. However, the steady state solutions depends not only on initial condition, but also on reaction rates. It is obvious that the quadratic equation is related with rate constants k_i. Understanding how variation of reaction rates affects steady or dynamic solutions is difficult to discern using linear or

nonlinear stability analysis. We therefore perform sensitivity analysis and uncertainty quantification to the system and show their effects.

Sensitivity analysis and uncertainty quantification of reaction rates and initial conditions and their impacts on steady state solutions

In Hockin-Mann's model, there are 16 reaction rates (shown in Table 8) that are derived through fitting computational results to empirical data. In order to investigate the uncertainties associated with these 16 reaction rates and depict their impacts on model predictions, the sparse grid probabilistic collocation method (SGPCM) [40, 41, 67] is utilized to generate the collocation points on the feasible parameter space of these 16 reaction rates, which are assumed to be random inputs with multivariate uniform distribution.

Sensitivity analysis of 16 data-fitted reaction rates

In this subsection, we apply two different stochastic sensitivity analysis methods, Morris method [46] based on Monte Carlo (MC) simulation and sparse grid collocation based on SGPCM approach, to rank the importance of the reaction rates on the total thrombin and study how the variation (uncertainty) in the total thrombin can be attributed to variations in the reaction rates as the inputs, i.e., systematically changing reaction rates in the model to determine the effects of such changes on the total thrombin concentration.

In applied statistics, the Morris method [46] for global sensitivity analysis is very efficient compared to other methods. We used the "Morris one at a time" (MOAT) module based on MC simulation performed by PSUADE [64], which is a software toolkit to facilitate the uncertainty analysis and design exploration. Figure 3 and Figure 4 show that the reaction rates k_{14}, k_{15} and k_{11} have more significant impact on the total thrombin synthesis compared with other fitted reaction rates. This result is consistent with the current understanding of coagulation cascade. k_{14} is the rate to form complex TF=VIIa=IX using TF=VIIa and IX. TF=VIIa=IX is subsequently disassociated to TF=VIIa and IXa with rate k_{15}. Moreover, k_{11} can control the production of TF=VIIa and Xa from TF=VIIa=Xa. The formation of the extrinsic factor Xa plays a key role in the total thrombin production, since prothrombinase catalyzes the conversion of zymogen prothrombin to thrombin.

Next, we used sparse grid probabilistic collocation methods [40,41,67], which can also result in sensitivity information, to rank sensitivities of these reaction rates and compare the results with that obtained by the Morris method [46]. Total variance of reaction rates on catalyzing thrombin was decomposed using analysis

of variance (ANOVA) technique as

$$v_{total} \;=\; \sum v_i \;+\; \sum v_{ij} \;+\; \sum v_{ijk} \;+\; \cdots,$$

where v_i is the variance of reaction rate i, v_{ij} is the covariance of rates i and j, and v_{ijk} is the covariance of rates i, j and k, etc.

This variance decomposition indicates the amount of information each reaction rate (v_i) contributes to the total thrombin production and determines how much of the variance of each reaction rate can be explained by the other reaction rates (v_{ij}). We use a network graph to present ranks of the importance of each reaction rate with respect to the total thrombin and also illustrate the interactions between 16 data-fitted reaction rates. See Figure 2 in which the radius of disks corresponding to reaction rate i is proportional to v_i/v_{total}, representing the normalized variance associated with reaction rate i. The lines between any pair of reaction rates i and j is proportional to v_{ij}/v_{total}, representing the correlation between that pair. The thicker the line is, the larger the correlation is. Figure 2 also helps us to avoid the mistake of ignoring reactions which have small variances associated with themselves, but large correlation with other reactions. It is obvious that k_{14} and k_{15} play major roles in generating thrombin. We note that only two-way interactions are shown in Figure 2, but higher order interactions can also be displayed using the same approach. We also note that, when the output is switched, the sensitivity is also switched. We applied variance decomposition and plotted the sensitivity analysis in Figure 5 when output changed to IXa=VIIIa and IXa=ATIII. Figure 5 shows that k_4 and k_{14} play important roles in generating IXa=VIIIa (x_{33}) and IXa=ATIII (x_{30}) respectively.

We conclude that the results obtained by the Morris design based on the MC simulations are consistent with the results based on SGPCM (Figure 2). Both of them show that the variances of k_{14}, k_{15} and k_{11} are larger, and that they are dominant reaction rates in generating the total thrombin.

Sensitivity analysis of initial conditions

From pervious study, we showed that initial concentrations of factors also contribute to steady states of the blood coagulation model. Here we performed sensitivity analysis of 10 non-zero initial concentrations of zymogen factors using SGPCM. These non-zero initial concentrations of zymogen factors are assumed to vary in 80%-120% of their normal values, and follow a uniformly distribution. The effects of initial conditions on the total thrombin synthesis is shown in Figure 6. Factor X (x_{15}) plays an important role in generating total thrombin and its cofactor Xa interacts with TFPI (x_{18}), which inhibits the thrombin production. Blood coagulation simulation is dependent on various model components such as reaction

rates, and initial concentrations. Sensitivity analysis of these reaction components can give a guidance to experimental variability in increasing and decreasing thrombin production.

Validation of uncertainty quantification method

The SGPCM approach can achieve much faster convergence than a classic MC method and it handles a larger number of uncertain parameters with relatively lower computational cost, when comparing sparse grids with full tensor products [40]. Here we utilized the MC simulations to verify accuracy of the SGPCM approach, which we employed to do uncertainty quantification. In Figure 7, we plotted the difference of the mean and variance of the total thrombin obtained by SGPCM (545 points) and MC (1000 points). The results (mean and variance of the total thrombin) obtained by the SGPCM approach is consistent with that of MC simulations. But the SGPCM is more efficient, and achieves faster convergence than MC. We used three different levels of sparse grid points (184 points, 1228 points and 6430 points) associated with 16 data-fitted reaction rates and treated the mean and variance of 6430 points as the "real solution". The absolute errors of the mean and variance for 34 variables are shown in Table 12 (Appendix E) which verifies the convergence of the SGPCM approach.

Propagation of uncertainty of reaction rates

Propagation of uncertainty of reaction rates in model solutions is studied in this section by using initial conditions described in [28]. The 16 data-fitted reaction rates are input variables and steady state concentrations of different factors are output variables. Runge-Kutta method is used to compute the time marching system on the sampling space of input variables. Figure 8 shows the mean and error bars of steady state solutions whose magnitudes are greater than 10^{-10} μm. Error bars show how the data are spread and encompass the lowest and highest values by using formula *mean* $\pm$ *standard deviation (SD)*, where *SD* is the average or typical difference between the data points and their mean. It is obvious that the steady state solutions we found are lying inside the intervals of Figure 8. The results of the mean and error bar for time marching simulations of undiluted whole blood triggered with 25 pM TF has been shown in Figure 9. Since it shows that thrombin production and consumption reach equilibrium by 700 seconds in Hockin-Mann's model, we studied the simulation over 700 seconds in time. Total thrombin is defined as thrombin (IIa) and meizothrombin (mIIa) with meizothrombin multiplied by a factor 1.2 because of meizothrombin's 20% greater activity toward substrates [28]. Figure 9 plots the mean and error bar of the total thrombin with total 545 sparse grid points for 16 data-fitted reaction rates. This prediction confidence interval of total

thrombin production is provided with the model as the quantification of the uncertainty.

Prediction of hemophilia therapy targeting factors VIII & IX

The sensitivity analysis provides threshold values for individual factors or reaction rate constants in controlling thrombin production. One application of our study is to examine women who are carriers of hemophilia diseases. Hemophilia is a group of hereditary genetic disorders that impair the body's ability to control blood clotting or coagulation, which is used to stop bleeding when a blood vessel is broken. There are two types of hemophilia diseases: one is factor VIII deficiency; and the other one is factor IX deficiency. These carriers contain a normal and defective gene for factor VIII or factor IX, and can present with a wide range of factor VIII or factor IX concentration levels in blood; as wide as 0-20% of concentrations in the blood of healthy individuals respectively. By knowing the threshold concentration of factor VIII or factor IX given the concentration levels of other factors, one can predict the level of thrombin production in case of bleeding, and subsequently determine if a carrier is at risk of bleeding disorder using our approach.

In this section, we show how factors VIII and IX quantitatively control the total thrombin concentration to identify individuals at risk of bleeding disorder for hemophiliac patients. We assume that the amounts of factors VIII and IX vary in ranges of 0-20% of their normal values. We also assume that the threshold of the total thrombin is 10% of its normal value. Below this level, people would have bleeding disorder. Other factors are assumed to be at their normal levels of concentration. We use uniformly distributed sampling points on factors VIII and IX, each factor having 100 points. The total thrombin is computed at each pair of sample points of factors VIII and IX by solving the time dependent system (see Appendix B). The total thrombin is compared to the assumed threshold value of total thrombin. Figure 10 shows that the threshold concentration of factor VIII is 4.7 % of its normal value, and that the threshold is increased when the concentration of factor IX increases. The histogram in Figure 11 shows the probability of the total thrombin above the threshold is 75.4% when factor VIII and factor IX vary. In this case, the risk of bleeding disorder is high (24.6%). The threshold of factor VIII is 4.7% of the normal value.

Furthermore, this analysis also identifies other factors that might lower the threshold concentration of factor VIII so that above threshold level of thrombin is produced to prevent from bleeding disorder. Based on the sensitivity analysis, we noticed that the threshold concentration of factor VIII would be lowered by increasing concentrations of the pro-coagulant factors that lead to produce total thrombin. Figures 2 and 6 show that the total thrombin concentration is activated by raising the value of reaction rate k_{14} and the initial concentration of factor X (x_{15}). Figure 12 shows that the total thrombin production is increased from

0.145 to 0.17 as k_{14} increases by 10% of the normal value. Increasing the value of reaction rate k_{14} is to activate factor IX to its active form IXa. This study is consistent with the study of the local measures [27], which are used with a pre-operative dose of raising the concentration level of factor IXa. In [27], factor IXa is increased 10% by using local measures of tranexamic acid solution, and excellent haemostasis is achieved for severe hemophiliac patients. In order to lower the threshold value of factor VIII in Figure 10, we let the rate of k_{14} and the initial concentration of factor X (x_{15}) vary in the range of 100-200% of their normal values. We again take 100 uniformly distributed sampling points in each of their parameter value spaces. The total thrombin is computed on the factor VIII and IX sampling space by time marching method. Figure 13 shows that the threshold of factor VIII is decreased to 3.3% by raising the value of reaction rate k_{14} and the initial concentration of factor X. Figure 14 shows the probability of bleeding disorder is also decreased to 17.7%. Thus it is possible by altering the activity the level of reaction rate k_{14}, and the initial concentration of factor X, one could reduce the level required of factor VIII to maintain normal hemostasis. Moreover, Factor IX is an important drug of haemostasis (see Table 9 for a sampling of current trials involving factor IX). Most trials involve the important factor IX. The lack of factor IX can produce bleeding episodes that cause damage of the bone, muscles, joints, and tissues. Control mechanisms involving factor IXa are common strategies in current anticoagulation conical therapies and clinical trials [43].

Discussion

This paper presents a general mathematical and computational framework which could also be used to identify effective drug therapy and predict its performance with confidence interval (Figure 1). First, an algorithm is developed to solve the steady state system with rank-deficiency derived from a mathematical model and establish a quantitative understanding of effects of reaction rates and initial conditions on the outputs of the model. This algorithm is the first one we are aware of that utilizes methods of numerical algebraic geometry to solve rank deficient systems. It can be used to analyze other dynamic systems with rank-deficiency. Moreover, our results show that the steady states depend not only on initial conditions but also on reaction rates. This algorithm enables us to find all solutions, among which the time marching method would not be able to solve the dynamical system with multiple equilibriums for given initial condition.

Second, we have developed a new technique to quickly solve the steady state system, as well as analyze the chemical reaction model using sensitivity analysis and uncertainty quantification methods. Finally, effective drug therapy is identified by comparing the importance ranking of the corresponding reaction rates obtained through sensitivity analysis study. We employ the numerical model to predict the performance of the most

effective drug therapy with confidence interval of corresponding thrombin production using SGPCM. Further analysis will be required to assess the effects of all parameters, such as reaction rates, using compressive sensing and optimization under uncertainty. Optimal control on the parameters for manipulating the total thrombin will be derived in our future works.

For Hockin-Mann's model, we explored the effects of 16 reaction rates whose values are obtained by fitting data and initial conditions. Both variance decomposition based sensitivity analysis and Morris design method were performed to rank the significance of the 16 uncertain reaction rates with respect to the total thrombin. Ranks of the importance of each reaction rate with respect to total thrombin concentration and the interactions between pair reactions are illustrated using a network graph (See Figure 5). Good agreement on the sensitivity ranking of the reaction rates is observed using both methods. SGPCM is employed to study the effect of the 16 uncertain reaction rates on the total thrombin concentration. The numerical results are consistent with the results obtained from classic Monte Carlo simulations. Additionally, the numerical results indicate that SGPCM can achieve much faster convergence than classic Monte Carlo method with much lower computational cost. (Figure 7)

Computational studies support the following three main conclusions:

- the steady states depend on the initial concentrations of factors and chemical reaction rates;
- our methods compute all steady states, which couldn't be founded by time marching method;
- among 16 fitted rate constants, the reaction rate k_{14} plays an important role in generating the total thrombin;
- the threshold concentration of factor VIII is controlled by k_{14} and factor X. This provides clinical guidance for the examination of bleeding disorder.

All "important" reaction rates, factors are listed in Box 2.

Box 2 Important reaction rates and factors

- k_{14} **and** k_{15}: are the most important reaction rates in generating IXa=VIIIa and IXa=ATIII respectively, eventually play important roles in generating the total thrombin;
- **factors VIII and IX**: deficiency causes two types of hemophilia diseases;
- k_{14} **and factor X**: control the threshold of factor VIII, and reduce the risk of bleeding disorder.

Although previous studies showed that experimental coagulation initiation at different levels of TF effects the total thrombin production. Our analysis investigates how altering both the initial concentrations of pro-

coagulant factors and values of reaction rate constants can effect thrombin production, and shows that k_{14} and k_{15} play a major role in generating the total thrombin since they directly control generation of the complex TF=VIIa=IX and thereafter control the generation of factor IXa. On the other hand, rates k_{37} and k_9, which consume TF=VIIa complex and factor X, prevent the total thrombin production. Moreover, k_4 activates, and k_{37} inhibits the role of k_{14}. In fact, larger values of k_4 yield more generation of TF=VIIa, which speeds up the thrombin production, and then activates the role of k_{14}. While k_{37} inhibits the thrombin production by consuming TF=VIIa to generate the complex TF=VIIa=Xa=TFPI, and then gives negative feedback to k_{14}. Furthermore, blocking k_{14} and k_{15} results in significant sensitivity shifts. Figure 15 shows that their affinities are predicted to be less important when values of k_{14} and k_{15} are reduced to 10% of their normal values. Conversely, the sensitivity of k_{23} related with factor VIIIa is found to increase. Our analysis also shows that the factor VIII plays an important role in the examination of bleeding disorder for women who are hemophilia carriers, and can vary within a wide range, namely, 20-80% of the normal value. Analysis of the threshold concentration of factor VIII can be used to predict if a carrier is at high risk of bleeding disorder. The threshold level for this particular factor in a patient would depend upon the activity rate and the concentration of all coagulation factors. The current common practice for hemophilia treatment is to replace the missing factor with exogenous material. If it is a human derived factor VIII, this carries the risk of spreading disease (as in the case of HIV and the high number of hemophiliacs who developed AIDS). One could provide recombinant proteins, but these are very expensive. Also recombinant proteins can induce the patient to generate an immune response to the foreign proteins and block their effectiveness. Thus, identifying the threshold value of factor VIII enables the use of small molecule inhibitors which are less likely to be immunogenic and should be cheaper than production of recombinant proteins. The sensitivity analysis could provide important clinical information to direct therapy for bleeding and thrombotic disorders.

Furthermore, the sensitivity analysis can identify new targets for hemorrhagic disorders. One approach to treat coagulation factor deficiencies is to replace the missing factor with exogenous material. Prophylactic use of exogenous material to prevent disease is very expensive and exogenous material is often just provided during the bleeding episodes but not for prophylactic purpose. Furthermore, the exogenous material may induce an immune response antagonizing the effect of replacement therapy. Sensitivity analysis may help identify other elements of the coagulation network where changes in activities may reduce the threshold concentration of the missing factors. Thus small molecule inhibitors or activators of the other elements (which are less likely to induce an immune response) can reduce the effects of the factor deficiency. This potentially may provide new therapeutic targets to treat coagulation deficiencies, and it also may be possible

to individualize the treatment for a specific patients based upon their level of coagulation components based on the guidance of the sensitivity analysis.

Methods

Overview of methods

Over the last decade, numerical algebraic geometry (see [38] and [59] for a review), which grew out of continuation methods for finding all isolated solutions of systems of nonlinear multivariate polynomials, became efficient and was applied to variety of problems. To approximate all isolated solutions of polynomial systems, numerical path following techniques have been proven reliable and efficient during the past two decades. In the 90's, homotopy methods were developed to exploit special structures of the polynomial system, in particular its sparsity. In numerical algebraic geometry, we apply and integrate homotopy continuation methods to describe solution components of polynomial systems. Moreover, we have been successful in the past in dealing with these types of problems, zebrafish model [24], necrotic core tumor growth model [25] and three dimensional tumor growth model [26]. In [25], we found multiple steady state solutions of the zebrafish model, which is hard to accomplish using classical numerical PDE algorithms. We applied homotopy continuation to free boundary problems discussed in [25, 26], and showed the efficiency of our algorithms. These studies provide the benefits of numerical algebraic geometry in studying nonlinear systems. All the computations are based on Bertini$^{\text{TM}}$ [4, 5], which is a software package in the field of numerical algebraic geometry that numerically compute all solutions of polynomial systems over $\mathbb{C}^n$. However, Bertini cannot be directly applied to a "deficient steady state system", which is defined as if some equations of a system can be expressed by a linear combination of other equations in this system. In other words, the Jacobian associated with the system is rank deficient at any given point. If the deficient system is also the steady state system derived from a differential equations system, then we call it as a "deficient steady state system".

There is rich literature on methods to study biochemical reaction networks, such as reaction network structures [17], Michaelis-Menten kinetics, linear kinetics and the rational parameterizations [62]. Specifically, [43] studies the fragility and robustness of the model and discusses the computationally derived points, correlation between the model simulation and experimental data, and computation of the Overall State Sensitivity Coefficients (OSSCs); [17] discusses the relationship between reaction network structure and the possibility of multiple equilibria based on computer algebra software; [62] uses a parameterization and transfers steady state system into a L algebraic equation. One common difficulty encountered by these methods is to deal with rank-deficient systems. To overcome this difficulty, we propose a new algorithm , which

can compute the steady states for rank-deficient systems and analyze stability of the solutions. Our results cannot be derived from any existing mathematical theories of biochemical reaction networks. The steady state solutions depend upon the initial condition and reaction rates. In Hockin-Mann's coagulation model, 16 reaction rate constants are obtained by data-fitting. Uncertainties associated with the TF pathway of blood coagulation due to uncertainty associated with these reaction rate constants remain unknown. We explore the significance of these data-fitted reaction rates by using uncertainty quantification and sensitivity analysis.

Sensitivity analysis is a powerful tool in ranking the importance of the random inputs and quantifying their interactions. The sensitivity approach in [52] uses a few sample points in a large parameter domain to rank the random inputs, which is a computationally efficient technique for a linear model. However, when the system has strong nonlinearities, more sample points covering the whole parameter domain have to be used. In sensitivity analysis, a common approach is changing One-At-a-Time (OAT), to see what effect this produces on the output. Sensitivity methods that use OAT design are sensitive approaches were the impact of changing the values of each factor is evaluated in turn. Randomly moved OAT as inputs is the most used screening method in sensitivity analysis. Many screening methods have been developed, e.g., Morris's method [11, 46, 55], Cotter's method [16], Andres' iterated fractional factorial method [3], Bettonvil's sequential bifurcation [7], and variance-based sensitivity analysis [55]. By using a sensitivity analysis framework to explore in the space of reaction rate parameters, we study the output statistics to understand how input uncertainties propagate through the Hockin-Mann's coagulation model and how Mann's model responds to variation in values of these simulation fitted reaction rates. The Morris method is utilized to show effects of reaction rates on generating the total thrombin. The total variance of total thrombin is decomposed by using Analysis Of Variance technique (ANOVA). We remark that the sensitivity analysis performed in the present paper can be extended to inverse modeling to calibrate model parameters to improve simulations. The relationships between the output responses and input parameters (response curves or surfaces) can also be used to develop reduced-order models for the subset of processes, which can then be used to perform more extensive uncertainty quantification of the complete model. Recently the probabilistic collocation method (PCM) has been applied for sensitivity analysis and can efficiently identify the sensitive parameters [53, 54]. In [39], the Multi-Element-PCM based sensitivity analysis method is developed, which is efficient and can achieve fast convergence compared to standard Monte Carlo (MC) based sensitivity analysis methods for cases with 20-100 random parameters. Moreover, PCM can be also used to speedup the convergence for uncertainty quantification introduced by Tatang and McRae [61]. Recently

Xiu and Hesthaven [67] have used Lagrange polynomial interpolation to construct high-order stochastic collocation methods. The properties of PCM were extensively studied in the past 10 years. In [6, 48, 49], the errors of integrating or interpolating functions with Sobolev regularity were analyzed for Smolyak constructions based on one-dimensional nested Clenshaw-Curtis rules. In [49], the degree of exactness of the Smolyak quadrature using Clenshaw-Curtis and Gaussian one-dimensional rules was investigated. In [67], the efficiency of Clenshaw-Curtis-based sparse grid stochastic collocation was demonstrated in comparison to other stochastic methods on an elliptic problem. In 2003, Gerstner and Griebel [21] introduced the dimension-adaptive tensor product quadrature method. In [20], sparse grid collocation schemes were applied to solving stochastic natural convection problems. In [22,44], an adaptive hierarchical sparse grid collocation algorithm has been developed. In this study, we apply the Sparse Grid Probabilistic Collocation Method (SGPCM) to study the uncertainty quantification process of Mann's model in a faster convergence rate. We validate our method by comparing results obtained by SGPCM and MC.

Sparse grid probabilistic collocation method

In this paper, we applied the uncertainty quantification method - SGPCM to achieve faster convergence in the uncertainty quantification process, compared with the classic MC simulations. The general procedure of the PCM approach is similar to that of the MC method except that different sampling points and corresponding weights are selected. The procedure of the PCM consists of the following of three main steps:

1. Generate N_c collocation points in probability space of random parameters as independent random inputs based on a quadrature formula;

2. Solve a deterministic problem at each collocation point;

3. Estimate the solution statistics using the corresponding quadrature rule,

$$\langle u(\boldsymbol{x},t)\rangle = \int_\Gamma u(\boldsymbol{x},t,\xi)\rho(\xi)d\xi \approx \sum_{k=1}^{N_c} u(\boldsymbol{x},t,\xi_k)w_k, \tag{3}$$

$$\sigma(u)(\boldsymbol{x},t) = \sqrt{\int_\Gamma (u(\boldsymbol{x},t,\xi)-\langle u\rangle)^2\rho(\xi)d\xi} \approx \sqrt{\sum_{k=1}^{N_c} u^2(\boldsymbol{x},t,\xi_k)w_k - \langle u\rangle^2}, \tag{4}$$

where $\rho(\xi)$ is the probability density function (PDF) of the random variable ξ, N_c is the number of quadrature points, $\{\xi_k\}$ is the set of quadrature points, and $\{w_k\}$ is the corresponding set of weights, which is the combination of quadrature weights in each random dimension. In the second step of the PCM, as for the MC method, any existing code can be used. Extensive reviews on the construction of quadrature formulas

may be found in [14, 15]. The Smolyak formula [56] is used to construct the collocation point set, which is a linear combination of tensor product formulas and the resulting point set has a significantly smaller number of points than the full tensor product set. Recently, Lagrange polynomial interpolation has been used [40, 41, 67] to construct high order stochastic collocation methods based on sparse grids using the Smolyak formula [56]. Such sparse grids do not depend as strong on the dimensionality of the random space as those more suitable for applications with high-dimensional random inputs. Detailed descriptions on building the collocation point set can be found in [40, 41, 67].

Global sensitivity analysis based on Polynomial Chaos Expansion (PCE)

Global sensitivity analysis can be obtained from PCEs in order to identify the dominant sources of uncertain parameters and their attributions. Generally, PCEs of a second-order stochastic processes with d number of independent random variables can be expressed as

$$g(x_1, \cdots, x_d) = \Sigma_{k=0}^{K-1} c_k \Psi_k(\mathbf{x}),$$

where $\mathbf{x} = (x_1, \cdots, x_d)$ is a set of independent random variables, $\Psi_k(\mathbf{x})$ are multidimensional orthogonal polynomials with regard to the inner product, and c_k are the deterministic polynomial chaos coefficients of g. Then the global sensitivity analysis based on variance decomposition is employed. Here the total variance is defined as

$$Var[g(\mathbf{x})] = \Sigma_{k>0} c_k^2 \|\Psi_k(\mathbf{x})\|^2,$$

where $\|\Psi_k(\mathbf{x})\|$ can be pre-computed, and c_k is calculated using the sparse grid probabilistic collocation method and the orthogonal property of polynomial chaos. Then the first-order (or main) effect sensitivity indices of S_i are

$$S_i \;=\; \frac{Var[\mathbb{E}\big(g(\mathbf{x}|x_i)\big)]}{Var[g(\mathbf{x})]} \;=\; \frac{\Sigma_{k\in\mathbb{I}_i}\; c_k^2 \|\Psi_k(\mathbf{x})\|^2}{\Sigma_{k>0}\; c_k^2 \|\Psi_k(\mathbf{x})\|^2},$$

where $\mathbb{I}_i$ is the set of bases with only x_i involved. S_i is the uncertainty contribution that is due to i-th parameter only. Similarly, the joint sensitivity indices can be written as

$$S_{ij} \;=\; \frac{Var[\mathbb{E}\big(g(\mathbf{x}|x_i, x_j)\big)]}{Var[g(\mathbf{x})]} - S_i - S_j \;=\; \frac{\Sigma_{k\in\mathbb{I}_{ij}}\; c_k^2 \|\Psi_k(\mathbf{x})\|^2}{\Sigma_{k>0}\; c_k^2 \|\Psi_k(\mathbf{x})\|^2},$$

where $\mathbb{I}_{ij}$ is the set of bases with only x_i and x_j involved. S_{ij} is the uncertainty contribution that is due to (i, j) parameter pair.

Method for solving rank-deficient polynomial system

We develop a numerical algorithm for studying the steady state system derived from the tissue factor-mediated coagulation pathway model introduced in [28] in this section. The coagulation cascade formulated in [28] is listed in Table 10 of Appendix A for the self-completeness of the paper. From this coagulation cascade, we get a mathematical model consisting of 34 ordinary differential equations (see Appendix B) with 42 rate constants which describe 27 independent equilibrium expressions listed in Table 10. Table 11 of Appendix A lists the notations to represent species in Table 10 used by ODEs in Appendix B. The corresponding steady state system, which is obtained by setting t-derivatives to be 0 for the ODE system, is a polynomial system with 34 variables. Unfortunately, this system cannot be solved directly by polynomial solvers such as Bertini [4] because of its rank-deficiency. In order to deal with the rank-deficiency, let us start with considering the rank of the polynomial system. From [59], the rank of a polynomial system equals to that of the Jacobian associated with the system at any random generic point. For our model, the rank of the steady state system is 24, which suggests that the system is not of full rank. An additional 10 linearly independent equations need to be added to the system in order to generate an augmented polynomial system. Here we introduce an idea of symbolic computation to determine these additional linear equations. Let $C(\mathbf{x}, \mathbf{k})$ denote monomial components of the steady state polynomial system, i.e., the multiplication of the rate constants and reactants,

$$\begin{aligned} C(\mathbf{x},\mathbf{k}) \;=\; & \Big(k_2x_1x_2, k_1x_3, k_4x_1x_4, k_3x_5, k_5x_5x_2, k_6x_6x_2, k_7x_7x_2, k_9x_5x_8, k_8x_9, k_{12}x_5x_6, k_{11}x_{10}, k_{14}x_5x_{11}, \\ & k_{13}x_{12}, k_{16}x_6x_{14}, k_{17}x_7x_{15}, k_{19}x_{16}x_{13}, k_{18}x_{17}, k_{21}x_{17}x_8, k_{20}x_{18}, k_{24}x_{16}, k_{23}x_{19}x_{20}, k_{25}x_{18}, k_{25}x_{17}, \\ & k_{26}x_7x_{21}, k_{28}x_6x_{22}, k_{27}x_{23}, k_{30}x_{23}x_{14}, k_{29}x_{24}, k_{32}x_{25}x_{23}, k_{34}x_6x_{26}, k_{33}x_{27}, k_{36}x_{10}x_{26}, k_{35}x_{28}, \\ & k_{37}x_5x_{27}, k_{38}x_6x_{29}, k_{39}x_{25}x_{29}, k_{40}x_{13}x_{29}, k_{41}x_7x_{29}, k_{42}x_5x_{29}, k_{10}x_9, k_{15}x_{12}, k_{22}x_{18}, k_{31}x_{24}\Big)^T, \end{aligned}$$

then the steady state polynomial system $f(\mathbf{x})$ can be expressed as

$$f(\mathbf{x}) = A \times C(\mathbf{x}, \mathbf{k}),$$

where A is a real valued matrix. Obviously, the rank of A is the same as the rank of the system $f(\mathbf{x})$. Since $rank(A) = 24$, there exists 24 linearly independent rows of A so that the other 10 rows of A can be represented by them (see Appendix C). Moreover, each row of A, say i-th row $A(i,:)$, is corresponding to i-th equation of $f(\mathbf{x})$ or $\frac{dx_i}{dt}$. For example, we have

$$A(24,:) = -A(21,:) - A(22,:) - A(23,:),$$

which means

$$\frac{dx_{24}}{dt} = -\frac{dx_{21}}{dt} - \frac{dx_{22}}{dt} - \frac{dx_{23}}{dt}$$
$$\Rightarrow \quad x_{24} + x_{21} + x_{22} + x_{23} = \text{Const}, \tag{5}$$

where Const is a constant determined by the initial condition. In this case, we can generate additional linear equations by the following algorithm.

Algorithm 1: Algorithm for generating linear equations

Input : The coefficient matrix $A_{n\times m}$.
Output: Linear equations generated.
for $i = 1 : n$ **do**
  determine if the row $A(i,:)$ is linearly independent upon B?
  if *true* **then**
    add $A(i,:)$ into B and add i into $\mathcal{I}_B$.
  else
    write $A(i,:)$ as a linear combination of the rows of B and insert the coefficients of B into $\mathcal{C}$.
    add i into $\mathcal{I}_{\mathcal{C}}$.
  end
end
for $i = 1 :$ *size of* $\mathcal{I}_{\mathcal{C}}$ **do**
  print $\frac{dx_{\mathcal{I}_{\mathcal{C}i}}}{dt} = \sum_j \mathcal{C}(i,j)\frac{dx_{\mathcal{I}_{\mathcal{B}j}}}{dt}$
end

For Mann's model, 10 linear equations can be generated and denoted as $L(x_1, x_2, \ldots, x_{34})$. Therefore, the augmented polynomial system becomes

$$F(x_1, x_2, \ldots, x_{34}) = \begin{pmatrix} f(x_1, x_2, \ldots, x_{34}) \\ L(x_1, x_2, \ldots, x_{34}) \end{pmatrix}. \tag{6}$$

Now we switch our attention to the computation of steady state solutions to system (6). Noticing that there are some simple polynomial equations such as f_{11}, f_{18}, f_{24}. We propose the following algorithm to simplify and to solve this rank-deficient polynomial system (RDPS).

Algorithm 2: Algorithm for solving RDPS(f)

Input : A set $f = \{f_1, \ldots, f_N\}$ of N polynomials, the linear system L.
Output: A set $g = \{f_1, \ldots, f_M\}$ of M simplified polynomials. A zero solution set $S = \{x_i | x_i = 0\}$.
Set $S = \{\emptyset\}$.
Call RDPS_iterative(f, L, S).

Algorithm 3: RDPS_iterative(f, L, S)

```
Input  : A polynomial set f = {f_1, ..., f_{N'}}, linear system L and solution set S
Output: true (success) or false
Set display_solution=true
if S does not satisfy L then
    return false
end
for i = 1 : N' do
    if f_i is single monomial then
        display_solution=false
        remove f_i from f, assume f_i = k_{s_i} x_{i_1} ··· x_{i_m}
        for j = 1 : m do
            add x_{i_j} into S, evaluate f as f' and L as L'
            if RDPS_iterative(f', L', S) then
                return true
            else
                remove x_{i_j} from S
            end
        end
    end
end
if display_solution then
    output f and S
    return true
end
return false
```

Author's contributions

WH, AS and ZX developed algorithms for steady states; WH, GL and ZX performed sensitivity and uncertainty to the model; WH, GL, ZX and ER analyze the therapy for bleeding disorder; AS and MA supervised the project. All authors read and approved the final manuscript.

Acknowledgements

We acknowledge supports by the Duncan Chair of the University of Notre Dame, NSF grants DMS-0800612, DMS-1115887, CCF-0515203 and CCF-0916606, NIH grants HL073750-01A1, 1R01GM100470-01, 1R01GM095959-01A1, the INGEN Initiative to Indiana University School of Medicine. GL also acknowledges support by the Applied Mathematics program of the U.S. DOE Office of Advanced Scientific Computing Research. Computations were performed using the computational resources of the National Energy Research Scientific Computing Center at Lawrence Berkeley National Laboratory and the William R. Wiley Environmental Molecular Sciences Laboratory (EMSL). EMSL is a DOE national scientific user facility located

at PNNL. The Pacific Northwest National Laboratory is operated by Battelle for the U.S. Department of Energy under Contract DE-AC05-76RL01830.

References

1. H.E. Assmus, R. Herwig, K.H. Cho and O. Wolkenhauer, Dynamics of biological systems: Role of systems biology in medical research, *Exp Rev Molec Diagn*, Vol. 6, pp. 891–902, 2006.

2. C.A. Arnaud, Systems biology's clinical future. *Chem Eng News*, Vol. 84, pp. 17–26, 2006.

3. T. H. Andres, W. C. Hajas, Using iterated fractional factorial design to screen parameters in sensitivity analysis of a probabilistic risk assessment model, *Proceedings of the joint international conference on mathematical methods and supercomputing in nuclear applications, Karlsruhe, Germany*, Vol. 2, pp. 328–337, 1993.

4. D.J. Bates, J.D. Hauenstein, A.J. Sommese, and C.W. Wampler, Bertini$^{\mathrm{TM}}$: Software for Numerical Algebraic Geometry. Available at bertini.nd.edu with permanent doi: dx.doi.org/10.7274/R0H41PB5.

5. D.J. Bates, J.D. Hauenstein, A.J. Sommese, and C.W. Wampler, *Numerically solving polynomial systems with Bertini, SIAM*, 2013.

6. V. Barthelmann, E. Novak, and K. Ritter, High dimensional polynomial interpolation on sparse grids, *Adv. Comput. Math.*, Vol. 12, pp. 273-288, 2000.

7. B. Bettonvil, Detection of important factors by sequential bifurcation, *Tilburg University Press*, Tilburg, 1990.

8. S. D. Bungay, P. A. Gentry, and R. D. Gentry. A mathematical model of lipid-mediated thrombin generation. *Mathematical Medicine and Biology*, Vol. 20, pp.105–129, 2003.

9. K. E. Brummel-Ziedins, R. L. Pouliot, K. G. Mann, Thrombin generation: phenotypic quantitation *J Thromb Haemost*, Vol. 2, pp. 281–288, 2004.

10. K. E. Brummel-Ziedins, M. F. Whelihan, M. Gissel, K. G. Mann, G. E. Rivard, Thrombin generation and bleeding in haemophilia A. *Haemophilia*, Vol. 15, pp. 1118-1125, 2009.

11. F. Campolongo, J. Cariboni, A. Saltelli, W. Schoutens, Enhancing the Morris method, *Sensitivity analysis of model output, Kenneth M. Hanson and Francois M. Hemez, eds., Los Alamos National Laboratory.*

12. S. Christley, Q. Nie and X. Xie. Incorporating Existing Network Information into Gene Network Inference, *PLoS ONE*, Vol. 4, e6799, 2009.

13. M. S. Chatterjee, W. S. Denney, H. Jing and S. L. Diamond. Systems biology of coagulation initiation: kinetics of thrombin generation in resting and activated human blood, *PLoS Computational Biology*, Vol. 6, Issue 9, e1000950, 2009.

14. R. Cools, Monomial cubature rules since 'stroud': A compilation, *J. Comput. Appl. Math.*, Vol. 48, pp. 309–326, 1993.

15. R. Cools, Monomial cubature rules since 'stroud': A compilation - part 2, *J. Comput. Appl. Math.*, Vol. 112, pp. 21–27, 1999.

16. S. C. Cotter, A screening design for factorial experiments iwth interactions, *Biometrika*, Vol. 66 , pp.317–320, 1991.

17. G. Craciun and M. Feinberg, Multiple Equilibria in Complex Chemical Reaction Networks: I. The Injectivity Property, *SIAM Journal on Applied Mathematics* , Vol. 65, pp. 1526–1546, 2005.

18. B. Engelmann Initiation of coagulation by tissue factor carriers in blood. *Blood Cells Mol. Dis.* Vol. 36, pp. 188–190, 2006.

19. A. L. Fogelson and N. Tania. Coagulation under flow: the influence of flow-mediated transport on the initiation and inhibition of coagulation. *Pathophysiology of Haemostasis and Thrombosis*, Vol. 34, pp. 91–108, 2005.

20. B. Ganapathysubramanian and N. Zabaras, Sparse grid collocation schemes for stochastic natural convection problems, *J. Comput. Phys.*, Vol. 225, pp. 652-685, 2007.

21. T. Gerstner and M. Griebel, Dimension-adaptive tensor-product quadrature, *Computing*, Vol. 71, pp. 65-87, 2003.

22. M. Griebel, Adaptive sparse grid multilevel methods for elliptic pdes based on finite differences, *Computing*, Vol. 61, pp. 151–180, 1998.

23. A. Hamadeh, M.A.J. Roberts, E. August, P.E. McSharry, P.K. Maini, J.P. Armitage, A. Papchristodoulou, Feedback control architecture & the bacterial chemotaxis network, *Plos. Comput. Biol.*, Vol. 7, 2011.

24. W. Hao, J.D. Hauenstein, B. Hu, Y. Liu, A.J. Sommese, and Y.-T. Zhang Multiple stable steady states of a reaction-diffusion model on zebrafish dorsal-ventral patterning *Discrete and Continuous Dynamical Systems - Series S*, Vol. 4, pp. 1413-1428, 2011.

25. W. Hao, J.D. Hauenstein, B. Hu, Y. Liu, A.J. Sommese, and Y.-T. Zhang, Bifurcation of steady-state solutions for a tumor model with a necrotic core, *Nonlinear Analysis Series B: Real World Applications*, Vol. 13, pp. 694–709, 2012.

26. W. Hao, J.D. Hauenstein, B. Hu, and A.J. Sommese, A three-dimensional steady-state tumor system, *Applied Mathematics and Computation*, Vol. 218, pp. 2661–2669, 2011.

27. I. D. Hewson, P. Makhmaloaf Management of third molar removal with a single dose of recombinant Factor IX (BeneFIX) and local measures in severe haemophilia B. *Aust. Dent. J.*, Vol. 55, pp. 322–324, 2010.

28. M. F. Hockin, K. C. Jones, S. J. Everse, and K. G. Mann. A Model for the Stoichiometric Regulation of Blood Coagulation. *J. Bio. Chem.*, Vol. 277, pp. 18322–18333, 2002.

29. K. A. Hogan, H. Weiler, S. T. Lord Mouse models in coagulation. *Thrombosis and Haemostasis.*, Vol. 87, pp. 563–74, 2002.

30. T. M. Hackeng, K. M. Seré, G. Tans and J. Rosing. Protein S stimulates inhibition of the tissue factor pathway by tissue factor pathway inhibitor. *PNAS*, Vol. 103, No. 9, pp. 3106–3111, 2006.

31. J. Jesty, E. Beltrami, and G. Willems. Mathematical analysis of a proteolytic positive-feedback loop: dependence of lag time and enzyme yields on the initial conditions and kinetic parameters. *Biochemistry*, Vol. 32, pp. 6266–6274, 1993.

32. K. C. Jones and K. G. Mann. A Model for the Tissue Factor Pathway to Thrombin. I. An Empirical Study. *J. Bio. Chem.*, Vol. 269, pp. 23357–23366, 1994.

33. K. C. Jones and K. G. Mann. A Model for the Tissue Factor Pathway to Thrombin. II. A Mathematical Simulation. *J. Bio. Chem.*, Vol. 269, pp. 23367–23373, 1994.

34. M.A. Khanin and V.V. Semenov. A mathematical model of the kinetics of blood coagulation. *J. Theor. Biol.*, Vol. 136, pp. 127–134, 1989.

35. A. L. Kuharsky, A. L. Fogelson, Surface-mediated control of blood coagulation: the role of binding site densities and platelet deposition. *Biophysical Journal*, Vol. 80, pp. 1050-1074, 2001.

36. M. P. Lambert, B. S. Sachais, M. A. Kowalska, Chemokines and thrombogenicity. *Thrombosis and Haemostasis.* Vol. 97, pp.2-9, 2007.

37. A. Lander, K. Gokoffski, F. Wan, Q. Nie, and A. Calof, Cell Lineages and the Logic of Proliferative Control. *PLoS Biology*, Vol. 7, e1000015, 2009.

38. T.Y. Li Numerical Solution of Polynomial Systems by Homotopy Continuation Methods in *Handbook of Numerical Analysis, Volume XI, Special Volume: Foundations of Computational Mathematics*, F. Cucker, ed., North-Holland, pp. 209–304, 2003.

39. G. Lin and G. E. Karniadakis, Sensitivity analysis and stochastic simulations of non-equilibrium plasma flow, *Int. J. Numer. Meth. Engng*, Vol. 80, pp. 738–766, 2009.

40. G. Lin and A. Tartakovsky, An efficient, high-order probabilistic collocation method on sparse grids for three-dimensional flow and solute transport in randomly heterogeneous porous media, *Advances in Water Resources*, Vol. 32, pp. 712–722, 2009.

41. G. Lin and A. Tartakovsky, Numerical studies of three-dimensional stochastic Darcy's equation and stochastic advection-diffusion-dispersion equation, *Journal of Scientific Computing*, Vol. 43, pp. 92-117, 2010.

42. K. Lo, S. Denney, and S. L. Diamond. Stochastic Modeling of Blood Coagulation Initiation. *Pathophysiology of Haemostasis and Thrombosis*, Vol. 34, pp. 80–90, 2005.

43. D. Luan, M. Zai, J. D. Varner, Computationally Derived Points of Fragility of a Human Cascade Are Consistent with Current Therapeutic Strategies, *PLoS Computational Biology*, Vol. 3, pp. 142-1359, 2007.

44. X. Ma and N. Zabaras, An adaptive hierarchical sparse grid collocation algorithm for the solution of stochastic differential equations, *J. Comput. Phys.*, Vol. 228, pp. 3084-3113, 2009.

45. T. Moore, C.S. Chou, Q. Nie, N.L. Jeon and T. M. Yi Robust Spatial Sensing of Mating Pheromone Gradients by Yeast Cells, *PLoS ONE*, Vol. 3 :e3865, 2008.

46. M. D. Morris, Factorial sampling plans for preliminary computational experiments, *Technometrics*, Vol. 33, pp.161–174, 1991.

47. Y. Nemerson, The tissue factor pathway of blood coagulation. *Semin. Hematol*, Vol. 29, pp. 170-176, 1992.

48. E. Novak and K. Ritter, High dimensional integration of smooth funcions over cubes, *Numer. Math.*, Vol. 75, pp. 79-97, 1996.

49. E. Novak and K. Ritter, Simple cubature formulas with high polynomial exactness, *Constr. Approx.*, Vol. 15, pp. 499-522, 1999.

50. Y. Pantazis, M. A. Katsoulakis, D.G. Vlachos. Parametric sensitivity analysis for biochemical reaction networks based on pathwise information theory, *BMC Bioinformatics*, Vol. 14, No. 311, pp. 1-19, 2013.

51. R. Paul, R. Wollman, W. T. Silkworth, I. K. Nardi, D. Cimini, A. Mogilner. Computer simulations predict that chromosome movements and rotations accelerate mitotic spindle assembly without compromising accuracy, *PNAS*, Vol. 106, pp. 15708-1513, 2009.

52. H. Rabitz, M. Kramer, D. Dacol, Sensitivity analysis in chemical kinetics, *Annu. Rev. Phys. Chem.* Vol. 34, pp. 419-461, 1983.

53. M. T. Reagan, H. N. Njam, R. G. Ghanem, O. M. Knio, Uncertainty quantification in reacting-flow simulations through non-intrusive spectral projection, *Comubstion and Flame* Vol. 132, pp. 545–555, 2003.

54. M. T. Reagan, H. N. Njam, R. G. Ghanem, O. M. Knio, Quantifying uncertainty in chemical systems modeling, *Int. J. Chem. Kin.*, Vol. 37, pp. 368–382, 2005.

55. A. Saltelli, K. Chan, M. Scott, Sensitivity analysis, *John Wiley & Sons Ltd, New York*, 2000.

56. S. Smolyak, Quadrature and interpolation formulas for tensor products of certain classes of functions, *Soviet Math. Dokl.*, Vol. 4, pp. 240–243, 1963.

57. O. Sozinova, Y. Jiang, D. Kaiser, and M. Alber, A Three-Dimensional Model of Myxobacterial Aggregation by Contact-mediated Interactions, *Proc. Natl. Acad. Sci.* Vol. 102, 11308-11312, 2005.

58. O. Sozinova, Y. Jiang, D. Kaiser, and M. Alber, A Three-Dimensional Modelof Fruiting Body Formation, *Proc. Natl. Acad. Sci.*, Vol. 103 pp. 17255-17259, 2006.

59. A. J. Sommese, C. W. Wampler, *The Numerical Solution of Systems of Polynomials Arising in Engineering and Science*, *World Scientific*, 2005.

60. P. Sommi, D. Cheerambathur, I. Brust-Mascher, A. Mogilner, Actomyosindependent cortical dynamics contributes to the prophase force-balance in the early Drosophila embryo, *PLoS One*, Vol. 6, e18366, 2011.

61. M. Tatang and G. McRae, Direct treatment of uncertainty in models of reaction and transport, *MIT Tech. Rep.*, 1994.

62. M. Thomson, J. Gunawardena, The Rational Parameterisation Theorem for Multisite Post-translational Modification Systems, *Journal of Theoretical Biology*, Vol. 261, pp. 626-636, 2009.

63. M.J. Tindall, S.L. Porter, P.K. Maini, J.P. Armitage, Modeling chemotaxis reveals the role of reversed phosphotransfer & a bi-functional kinase-phosphatase, *Plos. Comput. Biol.*, Vol.6, e1000896, 2010.

64. C. Tong The PSUADE Uncertainty Quantification Project. Avialable at *https://computation.llnl.gov/casc/uncertainty∼quantification/*.

65. V. C. Veer, K. G. Mann Regulation of tissue factor initiated thrombin generation by the stoichiometric inhibitors tissue factor pathway inhibitor, antithrombin-III, and heparin cofactor-II, *J Biol Chem.* Vol. 7, pp. 4367-4377, 1997.

66. Y. Wu, Y. Jiang, D. Kaiser and M. Alber, Periodic reversal of direction allows Myxobacteria to swarm, *Proc. Natl. Acad. Sci.* Vol. 106, pp. 1222-1227, 2009.

67. D. Xiu and J. S. Hesthaven, High order collocation methods for differential equations with random inputs, *SIAM J. Sci. Comput.*, Vol. 27, pp.1118-1139, 2005.

68. Z. Xu, J. Lioi, J. Mu, M. M. Kamocka, X. Liu, D. Z. Chen, E. D. Rosen and M. Alber, A Multiscale Model of Venous Thrombus Formation with Surface-Mediated Control of Blood Coagulation Cascade, *Biophysical Journal*, Vol. 98, pp.1723–1732 2010.

69. V. I. Zarnitsina, F. I. Ataullakhanov, A. I. Lobanov, and O. L. Morozova. Dynamics of spatially nonuniform patterning in the model of blood coagulation. *Chaos*, Vol. 11, pp. 57–70, 2001.

70. V. I. Zarnitsina, A. V. Pokhilko, and F. I. Ataullakhanov. A mathematical model for the spatio-temporal dynamics of intrinsic pathway of blood coagulation. I. The model description. *Thrombosis Research*, Vol. 84, pp. 225-236, 1996.

Tables

Table 1: Steady state solutions of Hockin-Mann's model [28] with initial conditions specified in [28]. See Table 11 in Appendix A for definition of variables.

Constant solutions	$x_1 = x_3 = x_5 = x_6 = x_7 = x_8 = x_9 = x_{10} = x_{12} = x_{18} = x_{23} = x_{24} = 0,$ $x_{25} = x_{27} = x_{28} = x_{29} = 0, x_{26} = 8.33 \times 10^{-10}, x_{30} = 5.33 \times 10^{-9}, x_{34} = 2.5 \times 10^{-11}$
Free variables	$x_4, x_{11}, x_{13}, x_{14}, x_{15}, x_{16}, x_{17}, x_{21}, x_{33}$
Linear expression	$x_2 = 3.3383 \times 10^{-9} - x_4, \quad x_{19} = x_{20} = 2.33 \times 10^{-10} - x_{15} - x_{16} - x_{17}$ $x_{22} = 6.67 \times 10^{-9} - x_{21}, \quad x_{31} = 4.67 \times 10^{-7} - x_{14} - x_{33}$ $x_{32} = 3 \times 10^{-8} - x_{11} - x_{13} - x_{17}$
Other equations	$k_{18}x_{17} + k_{25}x_{17} - k_{19}x_{16}x_{13} = 0, k_{18}x_{17} - k_{24}x_{16} + k_{23}x_{19}x_{20} - k_{19}x_{16}x_{13} = 0$

Table 2: Max eigenvalues for A_i

$\max(\rho(A_1))$	-4.3e-19	$\max(\rho(A_7))$	-7.1e-06	$\max(\rho(A_{13}))$	-4.9e-07
$\max(\rho(A_{18}))$	-1.1e-04	$\max(\rho(A_{24}))$	-1.1e-04	$\max(\rho(A_{30}))$	-1.1e-04
$\max(\rho(A_2))$	-1.1e-04	$\max(\rho(A_8))$	-1.1e-04	$\max(\rho(A_{14}))$	-1.1e-04
$\max(\rho(A_{19}))$	-1.1e-04	$\max(\rho(A_{25}))$	-7.1e-06	$\max(\rho(A_{31}))$	-1.1e-04
$\max(\rho(A_3))$	-1.1e-04	$\max(\rho(A_9))$	-1.1e-04	$\max(\rho(A_{15}))$	-1.1e-04
$\max(\rho(A_{20}))$	-1.1e-04	$\max(\rho(A_{26}))$	-1.8e-20	$\max(\rho(A_{32}))$	-1.1e-04
$\max(\rho(A_4))$	-4.3e-19	$\max(\rho(A_{10}))$	-3.6e-04	$\max(\rho(A_{16}))$	-1.1e-04
$\max(\rho(A_{21}))$	-1.1e-04	$\max(\rho(A_{27}))$	-6.4e-06	$\max(\rho(A_{33}))$	-1.1e-04
$\max(\rho(A_5))$	-2.3e-07	$\max(\rho(A_{11}))$	-1.1e-04	$\max(\rho(A_{17}))$	-1.1e-04
$\max(\rho(A_{22}))$	-1.1e-04	$\max(\rho(A_{28}))$	-1.1e-04	$\max(\rho(A_{34}))$	-1.1e-04
$\max(\rho(A_6))$	-1.5e-06	$\max(\rho(A_{12}))$	-1.1e-04		
$\max(\rho(A_{23}))$	-1.1e-04	$\max(\rho(A_{29}))$	-4.9e-07		

Table 3: Steady state solution by setting free variables be zeros in Table 1

zero solutions	$x_1 = x_3 = x_4 = x_5 = x_6 = x_7 = x_8 = x_9 = x_{10} = x_{11} = x_{12} = x_{14} = 0,$ $x_{15} = x_{18} = x_{21} = x_{23} = x_{24} = x_{25} = x_{27} = x_{28} = x_{29} = x_{32} = x_{33} = 0$
constant solutions	$x_2 = 3.3383 \times 10^{-9}, x_{22} = 6.67 \times 10^{-9}, x_{26} = 8.33 \times 10^{-10},$ $x_{30} = 5.33 \times 10^{-9}, x_{31} = 4.67 \times 10^{-7}, x_{34} = 2.5 \times 10^{-11}$
polynomial system	$3 \times 10^{-8} - x_{13} - x_{17} = 0$ $k_{18}x_{17} + k_{25}x_{17} - k_{19}x_{16}x_{13} = 0$ $k_{18}x_{17} - k_{24}x_{16} + k_{23}x_{19}x_{20} - k_{19}x_{16}x_{13} = 0$
linear equation	$x_{19} = x_{20} = 2.33 \times 10^{-10} - x_{16} - x_{17}$

Table 4: The relative difference of nonzero components of the steady state solution shown in 3 compared with the solution computed by time marching

x_i	relative difference	x_i	relative difference
x_2	4.67582e-08	x_{22}	7.70551e-09
x_{13}	1.84436e-08	x_{26}	3.94895e-09
x_{16}	7.40565e-08	x_{30}	8.09857e-08
x_{17}	4.58548e-08	x_{31}	6.09728e-08
x_{19}	7.49401e-08	x_{34}	4.63122e-08
x_{20}	7.49401e-08		

Table 5: Nonlinear stability of the steady state solution shown in Table 3

perturbation ϵ_n	$\|\tilde{x} - x_s\|$
$O(10^{-6})$	1.67733×10^{-5}
$O(10^{-7})$	1.33397×10^{-6}
$O(10^{-8})$	3.59671×10^{-7}

Table 6: Steady state solutions using initial conditions from [35]

Constant solutions	$x_1 = x_3 = x_5 = x_6 = x_7 = x_8 = x_9 = x_{10} = x_{12} = x_{18} = x_{23} = x_{24} = x_{25} = 0,$ $x_{27} = x_{28} = x_{29} = 0, x_{26} = 4.66 \times 10^{-9}, x_{30} = 3.25 \times 10^{-8}, x_{34} = 3.1 \times 10^{-10}$
Free variables	$x_4, x_{11}, x_{13}, x_{14}, x_{15}, x_{16}, x_{17}, x_{21}, x_{33}$
Linear expression	$x_2 = 6.45 \times 10^{-8} - x_4, \quad x_{19} = x_{20} = 4.31 \times 10^{-9} - x_{15} - x_{16} - x_{17}$ $x_{22} = 3.33 \times 10^{-8} - x_{21}, \quad x_{31} = 5.32 \times 10^{-6} - x_{14} - x_{33}$ $x_{32} = 5 \times 10^{-7} - x_{11} - x_{13} - x_{17}$
Other equations	$k_{18}x_{17} + k_{25}x_{17} - k_{19}x_{16}x_{13} = 0,$ $k_{18}x_{17} - k_{24}x_{16} + k_{23}x_{19}x_{20} - k_{19}x_{16}x_{13} = 0$

Table 7: Steady state solutions by setting free variables in Table 6 to zeros

zero solutions	$x_1 = x_3 = x_5 = x_6 = x_7 = x_8 = x_9 = x_{10} = x_{12} = x_{18} = x_{23} = x_{24} = 0,$ $x_{25} = x_{27} = x_{28} = x_{29} = 0 = x_4 = x_{11} = x_{14} = x_{15} = x_{21} = x_{32} = x_{33} = 0$
constant solutions	$x_2 = 6.45 \times 10^{-8}, x_{22} = 3.33 \times 10^{-8}, x_{26} = 4.66 \times 10^{-9}, x_{30} = 3.25 \times 10^{-8},$ $x_{31} = 5.32 \times 10^{-6}, x_{34} = 3.1 \times 10^{-10}$
polynomial system	$5 \times 10^{-7} - x_{13} - x_{17} = 0$ $k_{18}x_{17} + k_{25}x_{17} - k_{19}x_{16}x_{13} = 0$ $k_{18}x_{17} - k_{24}x_{16} + k_{23}x_{19}x_{20} - k_{19}x_{16}x_{13} = 0$
linear equation	$x_{19} = x_{20} = 4.31 \times 10^{-9} - x_{16} - x_{17}$

Table 8: Listing of reaction rates analyzed in Hockin-Mann's model. These values are obtained by fitting computational results to empirical data.

Rate no.	Lower bound	Upper bound
1	6.29×10^{-4}	3.1×10^{-3}
2	1.6×10^{5}	3.2×10^{6}
3	8.76×10^{-4}	3.1×10^{-3}
4	1.6×10^{5}	2.3×10^{7}
8	69 nm(PCPS)	4.35 nm(PCPS)
9	69 nm(PCPS)	4.35 nm(PCPS)
11	17	21
12	2×10^{7}	2.4×10^{7}
13	2.1	2.7
14	9×10^{6}	1.1×10^{7}
15	1.6	2
23	2×10^{4}	2.4×10^{4}
34	8×10^{5}	1×10^{6}
35	1×10^{-4}	1.2×10^{-4}
36	2.9×10^{8}	3.5×10^{8}
37	4.5×10^{7}	5.5×10^{7}

Table 9: Clinical trials information for factor IX, was assembled from http://ClinicalTrials.gov using the search terms factor IX, where both open and closed trials were accepted.

Trial Identifier	Condition	Intervention	Purpose
NCT00581126	Hemophilia B	Recombinant Factor IX Coagulation	To assess efficacy and safety of BeneFix for prophylaxis in "Short-term" therapy and on demand therapy for all bleeding episodes of subjects with hemophilia B
NCT00004801	Hemophilia B Factor IX Deficiency	monoclonal factor IX replacement therapy	Assess the safety and long-term efficacy of monoclonal factor IX concentrate in patients with factor IX deficiency.
NCT00000582	Blood Coagulation Disorders Hematologic Diseases Hemorrhagic Disorders	Factor IX	To test the efficacy of prothrombin complex concentrates (Factor IX) in the treatment of hemophiliac patients who had inhibitors to Factor VIII.
NCT01159210	Prothrombin Complex Factor Deficiency	Prothrombin complex concentrate	To assess the efficacy and safety of Prothromplex Total as a treatment for the immediate reversal of oral anticoagulant therapy with vitamin K antagonists in patients with acquired deficiency of prothrombin complex coagulation factors (II, VII, IX, X).

Figures

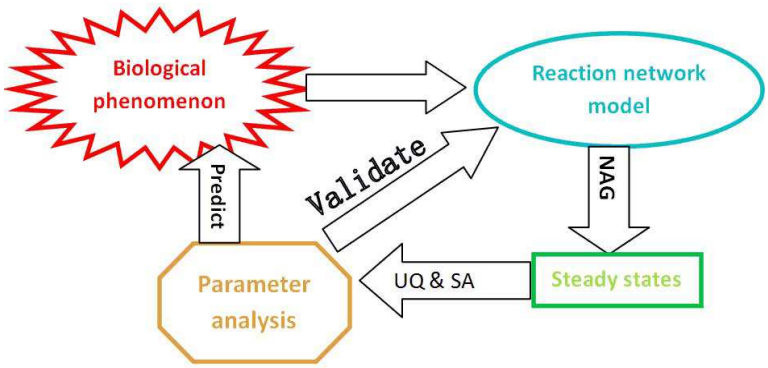

Figure 1: The general approach diagram of different stages in the analysis process: Numerical algebraic geometry (NAG) provides a numerical approach to compute all the steady states; Ranking importance of parameters, which is performed by uncertainty quantification (UQ) and sensitivity analysis (SA), validates the mathematical model and gives some medical prediction to the biological application.

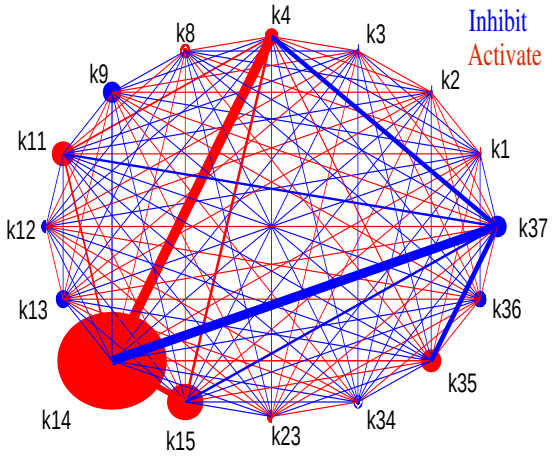

Figure 2: Network graph of importance of reaction rates and the interaction between pair reactions with respect to total thrombin. The radius of circles corresponding to reaction rate measures the rank of sensitivity while the width of lines of any pair of reaction rates represents rank of their co-sensitivity. The red color indicates that they play an activate role in generating thrombin production while the blue color means that they inhibit the generation of thrombin production. This figure shows that k_{14}, k_{15} and k_{11} are the most sensitive reaction rates in activating thrombin while k_{37} and k_9 inhibit thrombin production. Variance of k_4 and k_{14} can play a positive role in generation of thrombin production, however k_{37} and k_{14} inhibit generation of thrombin production.

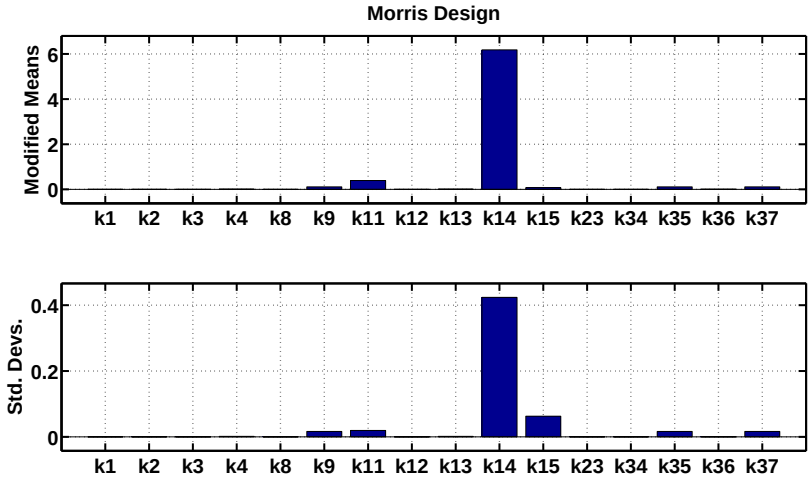

Figure 3: Modified means and standard deviations based sensitivity ranking of reaction rates with respect to the total thrombin using "Morris one at a time" method. Horizontal axis shows reaction rates. Vertical axis shows modified means and standard deviations respectively. This figure indicates that k_{14} has the largest modified mean and standard deviation. Therefore k_{14} is the most sensitive to thrombin production.

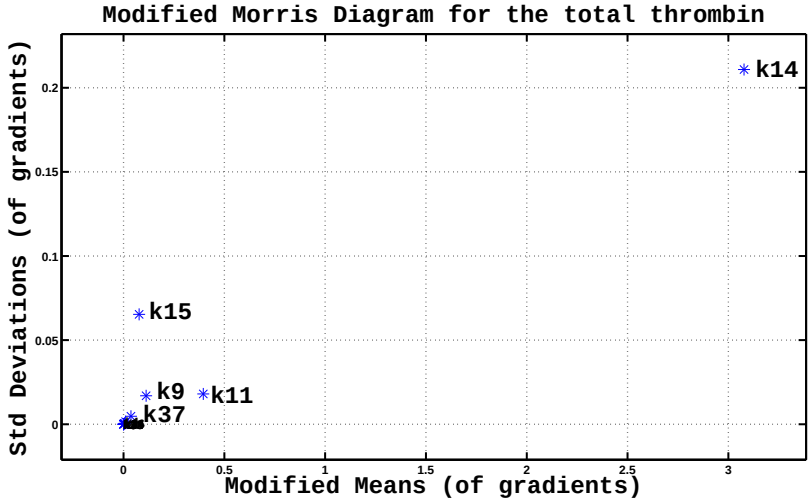

Figure 4: Modified Morris diagram on sensitivity ranking of reaction rates with respect to the total thrombin. Ranks of sensitivity for individual reaction rates are determined by their distance from the origin. From this figure, the five most sensitive reaction rates are k_{14}, k_{15}, k_{11}, k_9 and k_{37}. The other reaction rates cluster together due to the same magnitude of sensitivity.

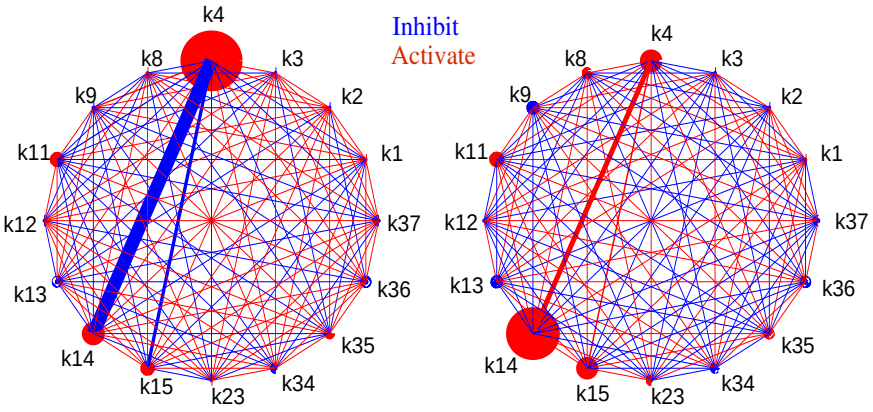

Figure 5: Network graph of importance of reaction rates and the interaction between reaction rates with respect to IXa=VIIIa (x_{33}) and IXa=ATIII (x_{30}) respectively. The same legend is used with Figure 1. This figure shows that the rank of sensitivity varices with respect to different output variables.

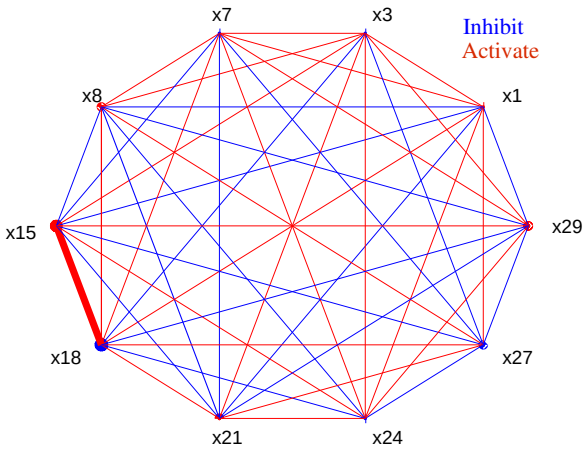

Figure 6: Network graph of importance of initial condition and the interaction between pair components with respect to total thrombin. See the legend in Figure 3. This figure shows that factor X (x_{15}) is the most sensitive reaction component in activating thrombin while TFPI (x_{18}) inhibits thrombin production. Moreover, their variance can play a positive role in generation of thrombin production.

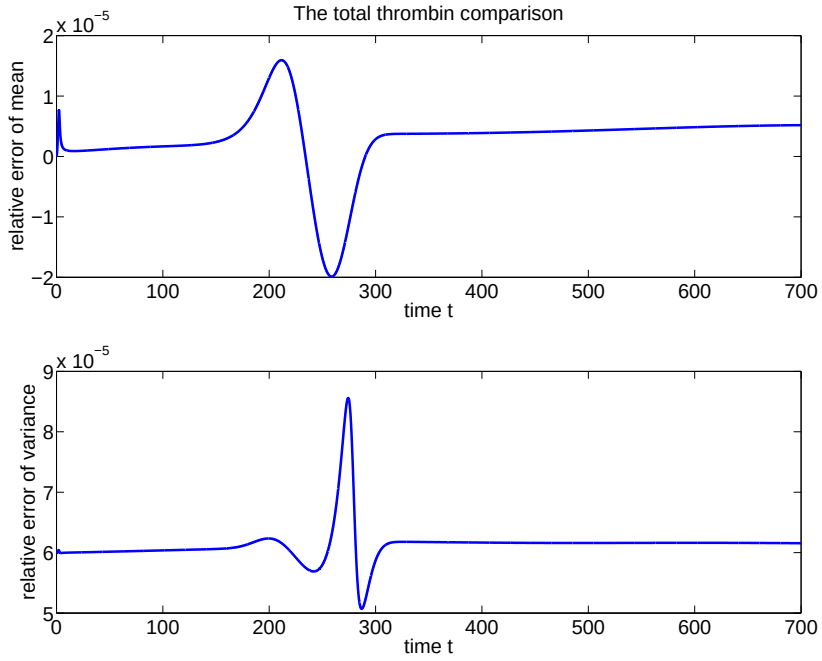

Figure 7: The Difference of mean and variance of the total thrombin obtained by SGPCM (545 points) and MC (1000 points). The figure shows that the results of two methods are same under small tolerance.

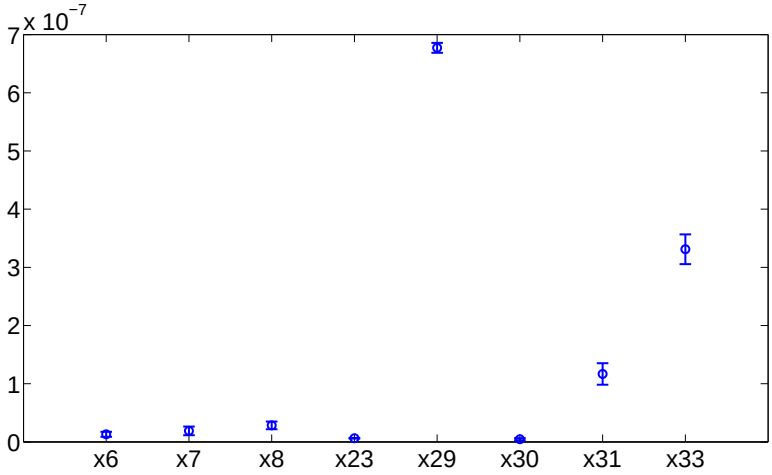

Figure 8: Mean and error bar of steady state solutions whose magnitude are greater than 10^{-10}. Horizontal axis is reaction rates. This figure shows confidence intervals of each reaction rates.

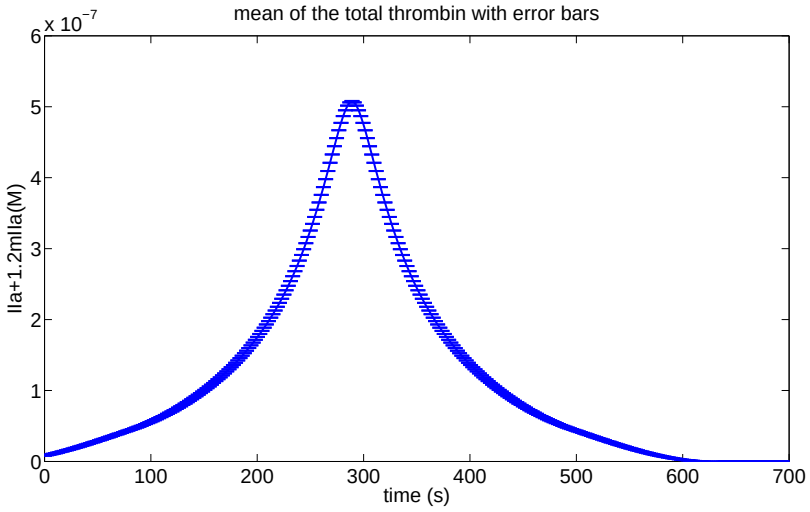

Figure 9: The mean and error bar of the total thrombin along the solution by time marching. Error bars show the confidence intervals of reaction rates along the curve.

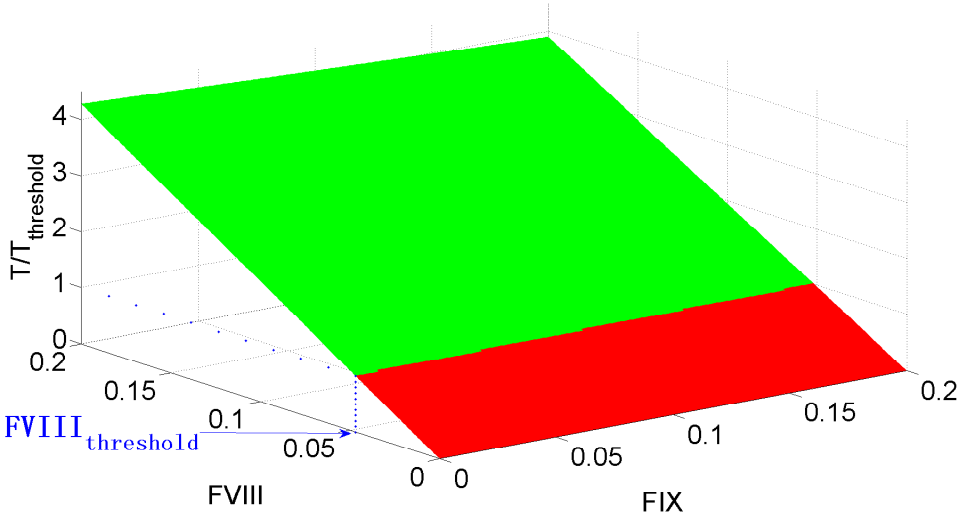

Figure 10: The total thrombin *v.s.* factors VIII (FVIII) and IX (FIX). $T_{threshold}$ stands for the threshold value of thrombin. The red portion of the plane means the total thrombin (T) is smaller than $T_{threshold}$ while the green portion means the total thrombin is greater than $T_{threshold}$. This figure shows that the threshold of factor VIII is 4.7 % of normal value, and that the total thrombin is greater than $T_{theshold}$ when factor VIII is greater than $FVIII_{theshold}$ regardless of factor IX concentration when it's in the assume range.

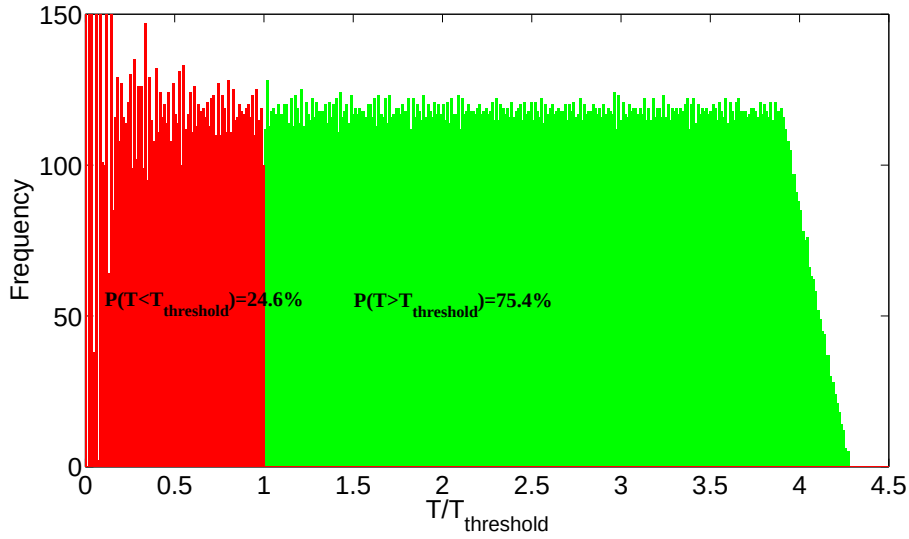

Figure 11: Histogram of the total thrombin. The probability that the total thrombin is greater than $T_{threshold}$ is 75.4%.

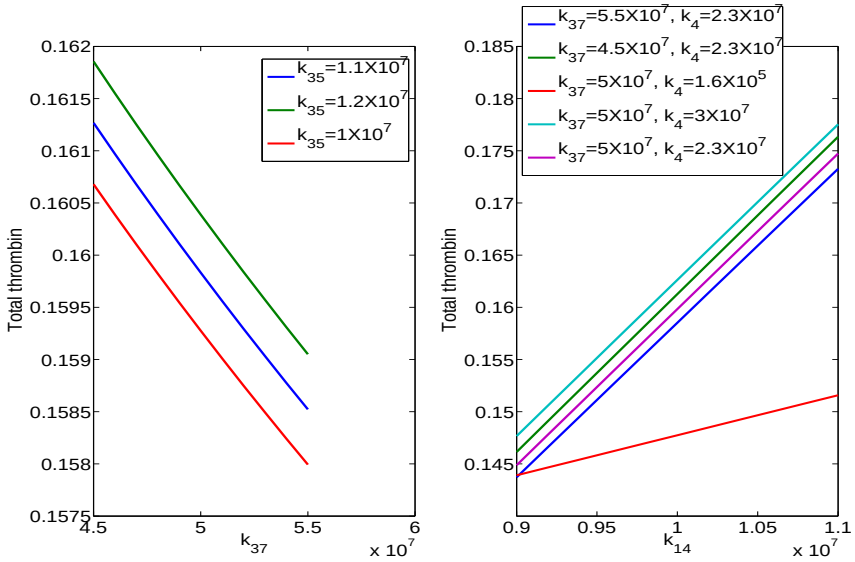

Figure 12: The total thrombin *v.s.* reaction rates k_{37} and k_{14}. k_{37} inhibits the generation of total thrombin as it increases. k_{35} plays a negative role in the effect of k_{37}. k_{14} activates the generation of total thrombin as it increases. k_{37} and k_4 play negative and positive roles in the effect of k_{14} respectively.

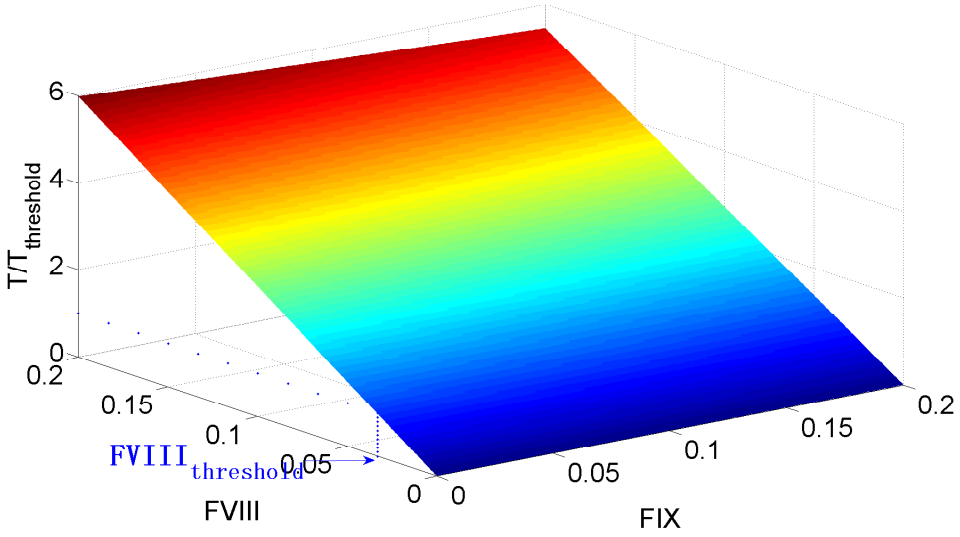

Figure 13: The mean of the total thrombin of sampling points of k_{14} and factor X, which vary from 100%-200% of their normal values. The color means the variance of the total thrombin. This figure shows that the threshold of factor VIII is decreased to 3.3% of normal value.

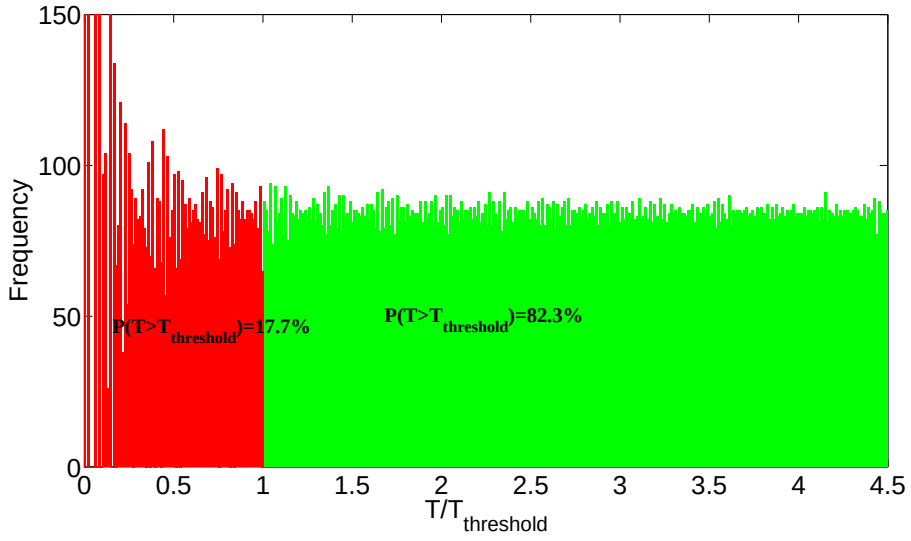

Figure 14: Histogram of the total thrombin as reaction rate k_{14} and factor X is introduced. The probability that the total thrombin is greater than $T_{threshold}$ is increased to 82.3%.

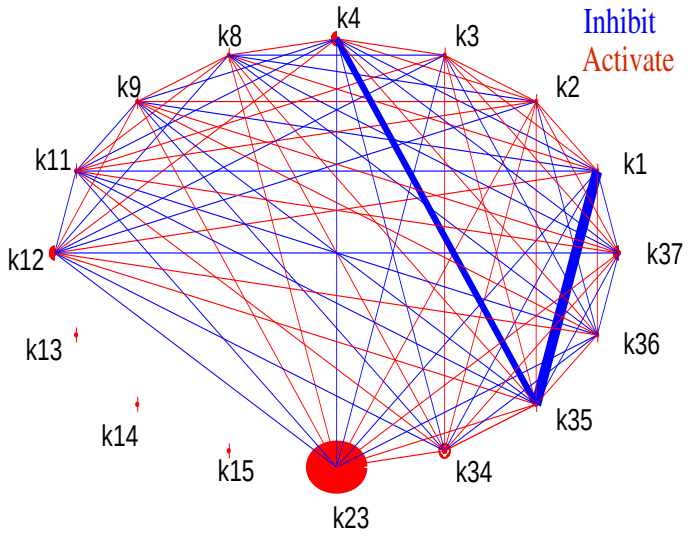

Figure 15: Network graph of importance of reaction rates and the interaction between pair components with respect to total thrombin when blocking k_{14} and k_{15} (their values are reduced by 90%). See the legend in Figure 1. This figure shows that the sensitivity shifts, i.e., reaction rate k_{23} becomes the most sensitive reaction rates in activating thrombin when k_{14} and k_{25} are blocked. Moreover, k_{13} plays no roles since chemical reaction with k_{13} is combined with k_{14} and k_{25}.

APPENDIX A

Chemical equations

Table 10: Chemical expressions for the coagulation cascade

Line	Chemical expressions
1	TF + VII $<1-2>$ TF=VII
2	TF + VIIa $<3-4>$ TF=VIIa
3	TF=VIIa + VII $-5>$ TF=VIIa + VIIa
4	Xa + VII $-6>$ Xa + VIIa
5	IIa + VII $-7>$ IIa + VIIa
6	TF=VIIa + X $<8-9>$ TF=VIIa=X $-10>$ TF=VIIa=Xa
7	TF=VIIa +Xa $<11-12>$ TF=VIIa=Xa
8	TF=VIIa + IX $<13-14>$ TF=VIIa=IX $-15>$ TF=VIIa + IXa
9	Xa + II $-16>$ Xa +IIa
10	IIa + VIII $-17>$ IIa + VIIIa
11	VIIIa + IXa $<18-19>$ IXa=VIIIa
12	IXa=VIIIa + X $<20-21>$ IXa=VIIIa=X $-22>$ IXa=VIIIa + Xa
13	VIIIa $<23-24>$ VIIIa_1· L + VIIIa_2
14	IXa=VIIIa=X $-25>$ VIIIa_1· L + VIIIa_2 + X +IXa
15	IXa=VIIIa $-25>$ VIIIa_1· L VIIIa_2 +IXa
16	IIa+ V $-26>$ IIa +Va
17	Xa + Va $<27-28>$ Xa=Va
18	Xa=Va + II $<29-30>$ Xa=Va=II $-31>$ Xa=Va + mIIa
19	mIIa+ Xa=Va $-32>$ IIa + Xa=Va
20	Xa + TFPI $<33-34>$ Xa=TFPI
21	TF=VIIa=Xa + TFPI $<35-36>$ TF=VIIa=Xa=TFPI
22	TF=VIIa + Xa=TFPI $-37>$ TF=VIIa=Xa=TFPI
23	Xa+ATIII $-38>$ Xa=ATIII
24	mIIa+ ATIII $-39>$ mIIa=ATIII
25	IXa + ATIII $-40>$ IXa=ATIII
26	IIa + ATIII $-41>$ IIa=ATIII
27	TF=VIIa + ATIII $-42>$TF=VIIa=ATIII

Table 11: Variables and Species

x_1	TF
x_2	IXa=VIIIa=X
x_3	VII
x_4	VIIIa_1· L
x_5	TF=VII
x_6	VIIIa_2
x_7	VIIa
x_8	V
x_9	TF=VIIa
x_{10}	Va
x_{11}	Xa
x_{12}	Xa=Va

x_{13}	IIa
x_{14}	Xa=Va=II
x_{15}	X
x_{16}	mIIa
x_{17}	TF=VIIa=X
x_{18}	TFPI
x_{19}	TF=VIIa=Xa
x_{20}	Xa=TFPI
x_{21}	IX
x_{22}	TF=VIIa=Xa=TFPI
x_{23}	TF=VIIa=IX
x_{24}	ATIII

x_{25}	IXa
x_{26}	Xa=ATIII
x_{27}	II
x_{28}	mIIa=ATIII
x_{29}	VIII
x_{30}	IXa=ATIII
x_{31}	VIIIa
x_{32}	IIa=ATIII
x_{33}	IXa=VIIIa
x_{34}	TF=VIIa=ATIII

APPENDIX B

Model equations

$$
\begin{aligned}
\frac{dx_1}{dt} &= -k_2x_1x_2 + k_1x_3 - k_4x_1x_4 + k_3x_5, \quad \frac{dx_2}{dt} = -k_2x_1x_2 + k_1x_3 - k_5x_5x_2 - k_6x_6x_2 - k_7x_7x_2 \\
\frac{dx_3}{dt} &= k_2x_1x_2 - k_1x_3, \qquad \frac{dx_4}{dt} = -k_4x_1x_4 + k_3x_5 + k_5x_5x_2 + k_6x_6x_2 + k_7x_7x_2 \\
\frac{dx_5}{dt} &= k_4x_1x_4 - k_3x_5 - k_9x_5x_8 + k_8x_9 - k_{12}x_5x_6 + k_{11}x_{10} - k_{14}x_5x_{11} + k_{13}x_{12} - k_{37}x_5x_{27} \\
&\quad -k_{42}x_5x_{29} + k_{15}x_{12} \\
\frac{dx_6}{dt} &= -k_{12}x_5x_6 + k_{11}x_{10} - k_{28}x_6x_{22} + k_{27}x_{23} - k_{34}x_6x_{26} + k_{33}x_{27} - k_{38}x_6x_{29} + k_{22}x_{18} \\
\frac{dx_7}{dt} &= k_{16}x_6x_{14} + k_{32}x_{25}x_{23} - k_{41}x_7x_{29}, \quad \frac{dx_8}{dt} = -k_9x_5x_8 + k_8x_9 - k_{21}x_{17}x_8 + k_{20}x_{18} + k_{25}x_{18} \\
\frac{dx_9}{dt} &= k_9x_5x_8 - k_8x_9 - k_{10}x_9, \qquad \frac{dx_{10}}{dt} = k_{12}x_5x_6 - k_{11}x_{10} - k_{36}x_{10}x_{26} + k_{35}x_{28} + k_{10}x_9 \\
\frac{dx_{11}}{dt} &= -k_{14}x_5x_{11} + k_{13}x_{12}, \qquad \frac{dx_{12}}{dt} = k_{14}x_5x_{11} - k_{13}x_{12} - k_{15}x_{12} \\
\frac{dx_{13}}{dt} &= -k_{19}x_{16}x_{13} + k_{18}x_{17} + k_{25}x_{18} + k_{25}x_{17} - k_{40}x_{13}x_{29} + k_{15}x_{12} \\
\frac{dx_{14}}{dt} &= -k_{16}x_6x_{14} - k_{30}x_{23}x_{14} + k_{29}x_{24} \\
\frac{dx_{15}}{dt} &= -k_{17}x_7x_{15}, \qquad \frac{dx_{16}}{dt} = k_{17}x_7x_{15} - k_{19}x_{16}x_{13} + k_{18}x_{17} - k_{24}x_{16} + k_{23}x_{19}x_{20} \\
\frac{dx_{17}}{dt} &= k_{19}x_{16}x_{13} - k_{18}x_{17} - k_{21}x_{17}x_8 + k_{20}x_{18} - k_{25}x_{17} + k_{22}x_{18} \\
\frac{dx_{18}}{dt} &= k_{21}x_{17}x_8 - k_{20}x_{18} - k_{25}x_{18} - k_{22}x_{18} \\
\frac{dx_{19}}{dt} &= \frac{dx_{20}}{dt} = k_{24}x_{16} - k_{23}x_{19}x_{20} + k_{25}x_{18} + k_{25}x_{17} \\
\frac{dx_{21}}{dt} &= -k_{26}x_7x_{21} \qquad \frac{dx_{22}}{dt} = k_{26}x_7x_{21} - k_{28}x_6x_{22} + k_{27}x_{23} \\
\frac{dx_{23}}{dt} &= k_{28}x_6x_{22} - k_{27}x_{23} - k_{30}x_{23}x_{14} + k_{29}x_{24} + k_{31}x_{24} \\
\frac{dx_{24}}{dt} &= k_{30}x_{23}x_{14} - k_{29}x_{24} - k_{31}x_{24}, \qquad \frac{dx_{25}}{dt} = -k_{32}x_{25}x_{23} - k_{39}x_{25}x_{29} + k_{31}x_{24} \\
\frac{dx_{26}}{dt} &= -k_{34}x_6x_{26} + k_{33}x_{27} - k_{36}x_{10}x_{26} + k_{35}x_{28} \\
\frac{dx_{27}}{dt} &= k_{34}x_6x_{26} - k_{33}x_{27} - k_{37}x_5x_{27}, \qquad \frac{dx_{28}}{dt} = k_{36}x_{10}x_{26} - k_{35}x_{28} + k_{37}x_5x_{27} \\
\frac{dx_{29}}{dt} &= -k_{38}x_6x_{29} - k_{39}x_{25}x_{29} - k_{40}x_{13}x_{29} - k_{41}x_7x_{29} - k_{42}x_5x_{29} \qquad \frac{dx_{30}}{dt} = k_{38}x_6x_{29} \\
\frac{dx_{31}}{dt} &= k_{39}x_{25}x_{29}, \qquad \frac{dx_{32}}{dt} = k_{40}x_{13}x_{29}, \qquad \frac{dx_{33}}{dt} = k_{41}x_7x_{29}, \qquad \frac{dx_{34}}{dt} = k_{42}x_5x_{29}, \qquad (7)
\end{aligned}
$$

where $k_i, i = 1, 2, ..., 42$ are constants, and $x_i, i = 1, 2, ..., 34$ are variables representing the species (see Table 11). The steady state system can be obtained by taking $t \to \infty$, i.e., $\frac{dx_i}{dt} = 0, \forall i$.

APPENDIX C

$$
\begin{aligned}
f_1 &= -k_4x_1x_4 + k_3x_5 \\
f_2 &= -k_5x_5x_2 - k_6x_6x_2 - k_7x_7x_2 \\
f_3 &= k_2x_1x_2 - k_1x_3 \\
f_4 &= -k_{12}x_5x_6 - k_{42}x_5x_{29} + k_4x_1x_4 - k_3x_5 + k_8x_9 - k_9x_5x_8 + k_{11}x_{10} - k_{37}x_5x_{27} \\
f_5 &= -k_{12}x_5x_6 - k_{34}x_6x_{26} + k_{11}x_{10} + k_{33}x_{27} - k_{38}x_6x_{29} + k_{22}x_{18} \\
f_6 &= k_{16}x_6x_{14} + k_{32}x_{25}x_{23} - k_{41}x_7x_{29} \\
f_7 &= -k_9x_5x_8 + k_8x_9 - k_{21}x_{17}x_8 + k_{20}x_{18} + k_{25}x_{18} \\
f_8 &= k_9x_5x_8 - k_8x_9 - k_{10}x_9 \\
f_9 &= k_{12}x_5x_6 - k_{11}x_{10} - k_{36}x_{10}x_{26} + k_{35}x_{28} + k_{10}x_9 \\
f_{10} &= -k_{14}x_5x_{11} + k_{13}x_{12} \\
f_{11} &= -k_{15}x_{12} \\
f_{12} &= -k_{19}x_{16}x_{13} + k_{18}x_{17} + k_{25}x_{18} + k_{25}x_{17} - k_{40}x_{13}x_{29} \\
f_{13} &= -k_{16}x_6x_{14} - k_{30}x_{23}x_{14} + k_{29}x_{24} \\
f_{14} &= -k_{17}x_7x_{15} \\
f_{15} &= -k_{19}x_{16}x_{13} + k_{18}x_{17} - k_{24}x_{16} + k_{23}x_{19}x_{20} \\
f_{16} &= k_{19}x_{16}x_{13} - k_{18}x_{17} - k_{21}x_{17}x_8 + k_{20}x_{18} - k_{25}x_{17} + k_{22}x_{18} \\
f_{17} &= k_{21}x_{17}x_8 - k_{20}x_{18} - k_{25}x_{18} - k_{22}x_{18} \\
f_{18} &= -k_{26}x_7x_{21} \\
f_{19} &= -k_{28}x_6x_{22} + k_{27}x_{23} \\
f_{20} &= k_{29}x_{24} - k_{30}x_{23}x_{14} + k_{31}x_{24} \\
f_{21} &= -k_{32}x_{25}x_{23} + k_{31}x_{24} \\
f_{22} &= -k_{34}x_6x_{26} + k_{33}x_{27} - k_{36}x_{10}x_{26} + k_{35}x_{28} \\
f_{23} &= k_{34}x_6x_{26} - k_{33}x_{27} - k_{37}x_5x_{27} \\
f_{24} &= k_{39}x_{25}x_{29},
\end{aligned}
$$

The next 10 rows can be expressed as:

$$
\begin{aligned}
A_4 &= A_1 - A_2 \\
A_{19} &= -A_{15} - A_{16} - A_{17} - A_{18} \\
A_{20} &= -A_{15} - A_{16} - A_{17} - A_{18} \\
A_{24} &= -A_{21} - A_{22} - A_{23} \\
A_{28} &= -A_{26} - A_{27} \\
A_{29} &= A_1 + A_3 + A_5 + A_6 + A_7 + A_8 + 2A_9 + 2A_{10} + A_{11} + 2A_{12} + A_{13} + A_{14} + A_{17} + 2A_{18} \\
&\quad -2A_{21} - 2A_{22} - A_{23} + A_{25} - 2A_{26} - A_{27} \\
A_{30} &= -A_6 - A_8 - A_9 - A_{10} - A_{18} + A_{21} + A_{22} + A_{26} \\
A_{32} &= -A_{11} - A_{12} - A_{13} - A_{17} \\
A_{33} &= -A_7 - A_{14} + A_{21} + A_{22} + A_{23} - A_{25} - A_{31} \\
A_{34} &= -A_1 - A_3 - A_5 - A_9 - A_{10} - A_{12} + A_{26} + A_{27},
\end{aligned}
$$

where $A_i,\ i = 1, 2, \ldots, 34$ represents the i-th row of A.

APPENDIX D

The linearized system of differential equation system shown in Appendix B:

$$
\begin{aligned}
{x^1}_{1t} &= -k_2{x^s}_1{x^1}_2 - k_2{x^1}_1{x^s}_2 + k_1{x^1}_3 - k_4{x^s}_1{x^1}_4 - k_4{x^1}_1{x^s}_4 + k_3{x^1}_5 \\
{x^1}_{2t} &= -k_2{x^s}_1{x^1}_2 - k_2{x^1}_1{x^s}_2 + k_1{x^1}_3 - k_5{x^s}_5{x^1}_2 - k_5{x^1}_5{x^s}_2 - k_6{x^s}_6{x^1}_2 - k_6{x^1}_6{x^s}_2 \\
&\quad -k_7{x^s}_7{x^1}_2 - k_7{x^1}_7{x^s}_2 \\
{x^1}_{3t} &= k_2{x^s}_1{x^1}_2 + k_2{x^1}_1{x^s}_2 - k_1{x^1}_3 \\
{x^1}_{4t} &= -k_4{x^s}_1{x^1}_4 - k_4{x^1}_1{x^s}_4 + k_3{x^1}_5 + k_5{x^s}_5{x^1}_2 + k_5{x^1}_5{x^s}_2 + k_6{x^s}_6{x^1}_2 + k_6{x^1}_6{x^s}_2 \\
&\quad +k_7{x^s}_7{x^1}_2 + k_7{x^1}_7{x^s}_2 \\
{x^1}_{5t} &= k_8{x^1}_9 + k_4{x^s}_1{x^1}_4 + k_4{x^1}_1{x^s}_4 + k_{13}{x^1}_{12} + k_{11}{x^1}_{10} - k_3{x^1}_5 - k_9{x^s}_5{x^1}_8 - k_9{x^1}_5{x^s}_8 \\
&\quad -k_{12}{x^s}_5{x^1}_6 - k_{12}{x^1}_5{x^s}_6 - k_{14}{x^s}_5{x^1}_{11} - k_{14}{x^1}_5{x^s}_{11} - k_{37}{x^s}_5{x^1}_{27} - k_{37}{x^1}_5{x^s}_{27} \\
&\quad -k_{42}{x^s}_5{x^1}_{29} - k_{42}{x^1}_5{x^s}_{29} + k_{15}{x^1}_{12} \\
{x^1}_{6t} &= k_{33}{x^1}_{27} + k_{27}{x^1}_{23} + k_{22}{x^1}_{18} + k_{11}{x^1}_{10} - k_{12}{x^s}_5{x^1}_6 - k_{12}{x^1}_5{x^s}_6 - k_{28}{x^s}_6{x^1}_{22} \\
&\quad -k_{28}{x^1}_6{x^s}_{22} - k_{34}{x^s}_6{x^1}_{26} - k_{34}{x^1}_6{x^s}_{26} - k_{38}{x^s}_6{x^1}_{29} - k_{38}{x^1}_6{x^s}_{29} \\
{x^1}_{7t} &= k_{16}{x^s}_6{x^1}_{14} + k_{16}{x^1}_6{x^s}_{14} + k_{32}{x^s}_{25}{x^1}_{23} + k_{32}{x^1}_{25}{x^s}_{23} - k_{41}{x^s}_7{x^1}_{29} - k_{41}{x^1}_7{x^s}_{29} \\
{x^1}_{8t} &= -k_9{x^s}_5{x^1}_8 - k_9{x^1}_5{x^s}_8 + k_8{x^1}_9 - k_{21}{x^s}_{17}{x^1}_8 - k_{21}{x^1}_{17}{x^s}_8 + k_{20}{x^1}_{18} + k_{25}{x^1}_{18} \\
{x^1}_{9t} &= k_9{x^s}_5{x^1}_8 + k_9{x^1}_5{x^s}_8 - k_8{x^1}_9 - k_{10}{x^1}_9 \\
{x^1}_{10t} &= k_{12}{x^s}_5{x^1}_6 + k_{12}{x^1}_5{x^s}_6 - k_{11}{x^1}_{10} - k_{36}{x^s}_{10}{x^1}_{26} - k_{36}{x^1}_{10}{x^s}_{26} + k_{35}{x^1}_{28} + k_{10}{x^1}_9 \\
{x^1}_{11t} &= -k_{14}{x^s}_5{x^1}_{11} - k_{14}{x^1}_5{x^s}_{11} + k_{13}{x^1}_{12} \\
{x^1}_{12t} &= k_{14}{x^s}_5{x^1}_{11} + k_{14}{x^1}_5{x^s}_{11} - k_{13}{x^1}_{12} - k_{15}{x^1}_{12} \\
{x^1}_{13t} &= -k_{19}{x^s}_{16}{x^1}_{13} - k_{19}{x^1}_{16}{x^s}_{13} + k_{18}{x^1}_{17} + k_{25}{x^1}_{18} + k_{25}{x^1}_{17} - k_{40}{x^s}_{13}{x^1}_{29} - k_{40}{x^1}_{13}{x^s}_{29} \\
&\quad +k_{15}{x^1}_{12} \\
{x^1}_{14t} &= -k_{16}{x^s}_6{x^1}_{14} - k_{16}{x^1}_6{x^s}_{14} - k_{30}{x^s}_{23}{x^1}_{14} - k_{30}{x^1}_{23}{x^s}_{14} + k_{29}{x^1}_{24} \\
{x^1}_{15t} &= -k_{17}({x^s}_7{x^1}_{15} + {x^1}_7{x^s}_{15}) \\
{x^1}_{16t} &= k_{17}{x^s}_7{x^1}_{15} + k_{17}{x^1}_7{x^s}_{15} - k_{19}{x^s}_{16}{x^1}_{13} - k_{19}{x^1}_{16}{x^s}_{13} + k_{18}{x^1}_{17} - k_{24}{x^1}_{16} + k_{23}{x^s}_{19}{x^1}_{20} \\
&\quad +k_{23}{x^1}_{19}{x^s}_{20} \\
{x^1}_{17t} &= k_{19}{x^s}_{16}{x^1}_{13} + k_{19}{x^1}_{16}{x^s}_{13} - k_{18}{x^1}_{17} - k_{21}{x^s}_{17}{x^1}_8 - k_{21}{x^1}_{17}{x^s}_8 + k_{20}{x^1}_{18} - k_{25}{x^1}_{17} \\
&\quad +k_{22}{x^1}_{18}
\end{aligned}
$$

$$
\begin{aligned}
{x^1}_{18t} &= k_{21}{x^s}_{17}{x^1}_8 + k_{21}{x^1}_{17}{x^s}_8 - k_{20}{x^1}_{18} - k_{25}{x^1}_{18} - k_{22}{x^1}_{18} \\
{x^1}_{19t} &= k_{24}{x^1}_{16} - k_{23}{x^s}_{19}{x^1}_{20} - k_{23}{x^1}_{19}{x^s}_{20} + k_{25}{x^1}_{18} + k_{25}{x^1}_{17} \\
{x^1}_{20t} &= k_{24}{x^1}_{16} - k_{23}{x^s}_{19}{x^1}_{20} - k_{23}{x^1}_{19}{x^s}_{20} + k_{25}{x^1}_{18} + k_{25}{x^1}_{17} \\
{x^1}_{21t} &= -k_{26}({x^s}_7{x^1}_{21} + {x^1}_7{x^s}_{21}) \\
{x^1}_{22t} &= k_{26}{x^s}_7{x^1}_{21} + k_{26}{x^1}_7{x^s}_{21} - k_{28}{x^s}_6{x^1}_{22} - k_{28}{x^1}_6{x^s}_{22} + k_{27}{x^1}_{23} \\
{x^1}_{23t} &= k_{28}{x^s}_6{x^1}_{22} + k_{28}{x^1}_6{x^s}_{22} - k_{27}{x^1}_{23} - k_{30}{x^s}_{23}{x^1}_{14} - k_{30}{x^1}_{23}{x^s}_{14} + k_{29}{x^1}_{24} + k_{31}{x^1}_{24} \\
{x^1}_{24t} &= k_{30}{x^s}_{23}{x^1}_{14} + k_{30}{x^1}_{23}{x^s}_{14} - k_{29}{x^1}_{24} - k_{31}{x^1}_{24} \\
{x^1}_{25t} &= -k_{32}{x^s}_{25}{x^1}_{23} - k_{32}{x^1}_{25}{x^s}_{23} - k_{39}{x^s}_{25}{x^1}_{29} - k_{39}{x^1}_{25}{x^s}_{29} + k_{31}{x^1}_{24} \\
{x^1}_{26t} &= -k_{34}{x^s}_6{x^1}_{26} - k_{34}{x^1}_6{x^s}_{26} + k_{33}{x^1}_{27} - k_{36}{x^s}_{10}{x^1}_{26} - k_{36}{x^1}_{10}{x^s}_{26} + k_{35}{x^1}_{28} \\
{x^1}_{27t} &= k_{34}{x^s}_6{x^1}_{26} + k_{34}{x^1}_6{x^s}_{26} - k_{33}{x^1}_{27} - k_{37}{x^s}_5{x^1}_{27} - k_{37}{x^1}_5{x^s}_{27} \\
{x^1}_{28t} &= k_{36}{x^s}_{10}{x^1}_{26} + k_{36}{x^1}_{10}{x^s}_{26} - k_{35}{x^1}_{28} + k_{37}{x^s}_5{x^1}_{27} + k_{37}{x^1}_5{x^s}_{27} \\
{x^1}_{29t} &= -k_{42}{x^s}_5{x^1}_{29} - k_{42}{x^1}_5{x^s}_{29} - k_{38}{x^s}_6{x^1}_{29} - k_{38}{x^1}_6{x^s}_{29} - k_{41}{x^s}_7{x^1}_{29} \\
&\quad -k_{41}{x^1}_7{x^s}_{29} - k_{40}{x^s}_{13}{x^1}_{29} - k_{40}{x^1}_{13}{x^s}_{29} - k_{39}{x^s}_{25}{x^1}_{29} - k_{39}{x^1}_{25}{x^s}_{29} \\
{x^1}_{30t} &= k_{38}({x^s}_6{x^1}_{29} + {x^1}_6{x^s}_{29}) \\
{x^1}_{31t} &= k_{39}({x^s}_{25}{x^1}_{29} + {x^1}_{25}{x^s}_{29}) \\
{x^1}_{32t} &= k_{40}({x^s}_{13}{x^1}_{29} + {x^1}_{13}{x^s}_{29}) \\
{x^1}_{33t} &= k_{41}({x^s}_7{x^1}_{29} + {x^1}_7{x^s}_{29}) \\
{x^1}_{34t} &= k_{42}({x^s}_5{x^1}_{29} + {x^1}_5{x^s}_{29})
\end{aligned}
$$

Appendix E

Table 12: Convergence study of SGPCM

Abs. Err.				
	Mean		Variance	
No.	184	1228	184	1228
1	2.285678e-004	6.276008e-005	1.414116e+000	5.270631e-001
2	3.528170e-003	9.790568e-004	1.421438e+000	5.282797e-001
3	1.117445e-002	3.058945e-003	1.451133e+000	5.334394e-001
4	1.737843e-004	4.822458e-005	1.421425e+000	5.282775e-001
5	8.828347e-003	2.389501e-003	1.486561e+000	5.391973e-001
6	1.988338e-002	5.317003e-003	1.566493e+000	5.520586e-001
7	4.584148e-003	1.255587e-003	1.427882e+000	5.293661e-001
8	2.048073e-004	5.578918e-005	1.454606e+000	5.339573e-001
9	3.396093e-003	9.241881e-004	1.424554e+000	5.287619e-001
10	3.256174e-003	8.869390e-004	1.423624e+000	5.286163e-001
11	8.412776e-006	2.279950e-006	1.480436e+000	5.382099e-001
12	8.808674e-003	2.384262e-003	1.486394e+000	5.391702e-001
13	8.277039e-003	2.243433e-003	1.479954e+000	5.381284e-001
14	3.103763e-003	8.465279e-004	1.443678e+000	5.320069e-001
15	7.814273e-003	2.193114e-003	1.426201e+000	5.286388e-001
16	1.328375e-002	3.739625e-003	1.415327e+000	5.270061e-001
17	9.094976e-003	2.458848e-003	1.490370e+000	5.397825e-001
18	8.172212e-003	2.212621e-003	1.483100e+000	5.386074e-001
19	2.363583e-003	6.446736e-004	1.460426e+000	5.347973e-001
20	2.363583e-003	6.446736e-004	1.460426e+000	5.347973e-001
21	7.814273e-003	2.193114e-003	1.426201e+000	5.286388e-001
22	7.593356e-003	2.131857e-003	1.425644e+000	5.288239e-001
23	2.706446e-003	7.513140e-004	1.429067e+000	5.297737e-001
24	1.078126e-002	2.958615e-003	1.431272e+000	5.298548e-001
25	9.639244e-003	2.646268e-003	1.426693e+000	5.291310e-001
26	3.609443e-004	9.730916e-005	1.492187e+000	5.400877e-001
27	1.019074e-002	2.748554e-003	1.499708e+000	5.413532e-001
28	2.549383e-003	6.949484e-004	1.420171e+000	5.280515e-001
29	5.662490e-004	1.541640e-004	1.448082e+000	5.327725e-001
30	9.960178e-003	2.677646e-003	1.508239e+000	5.426681e-001
31	2.958200e-003	8.078085e-004	1.445202e+000	5.322928e-001
32	7.845463e-003	2.126566e-003	1.478513e+000	5.378746e-001
33	2.120963e-003	5.769229e-004	1.427220e+000	5.293214e-001
34	8.380451e-003	2.269408e-003	1.483615e+000	5.387117e-001